

## More About This Article

---

Additional resources and features associated with this article are available within the HTML version:

- Supporting Information
- Access to high resolution figures
- Links to articles and content related to this article



- Copyright permission to reproduce figures and/or text from this article

[View the Full Text HTML](#)



## The Conformations of 13-Vertex $ML_2C_2B_{10}$ Metallocarboranes: Experimental and Computational Studies

Kelly J. Dalby,<sup>†</sup> David Ellis,<sup>†</sup> Stefan Erhardt,<sup>†</sup> Ruaraidh D. McIntosh,<sup>†</sup>  
Stuart A. Macgregor,<sup>\*,†</sup> Karen Rae,<sup>†</sup> Georgina M. Rosair,<sup>†</sup> Volker Settels,<sup>†</sup>  
Alan J. Welch,<sup>\*,†</sup> Bruce E. Hodson,<sup>‡</sup> Thomas D. McGrath,<sup>\*,‡</sup> and  
F. Gordon A. Stone<sup>‡</sup>

Contribution from the School of Engineering and Physical Sciences, Heriot-Watt University, Edinburgh EH14 4AS, U.K., and Department of Chemistry and Biochemistry, Baylor University, Waco, Texas 76798-7348

Received October 27, 2006; E-mail: a.j.welch@hw.ac.uk

**Abstract:** The dicosahedral metallocarboranes 4,4-(PMe<sub>2</sub>Ph)<sub>2</sub>-4,1,6-*closo*-PtC<sub>2</sub>B<sub>10</sub>H<sub>12</sub>, 4,4-(PMe<sub>2</sub>Ph)<sub>2</sub>-4,1,10-*closo*-PtC<sub>2</sub>B<sub>10</sub>H<sub>12</sub>, and [N(PPh<sub>3</sub>)<sub>2</sub>][4,4-cod-4,1,10-*closo*-RhC<sub>2</sub>B<sub>10</sub>H<sub>12</sub>] were prepared by reduction/metalation of either 1,2-*closo*-C<sub>2</sub>B<sub>10</sub>H<sub>12</sub> or 1,12-*closo*-C<sub>2</sub>B<sub>10</sub>H<sub>12</sub>. All three species were fully characterized, with a particular point of interest of the latter being the conformation of the {ML<sub>2</sub>} fragment relative to the carborane ligand face. Comparison with conformations previously established for six other ML<sub>2</sub>C<sub>2</sub>B<sub>10</sub> species of varying heteroatom patterns (4,1,2-*MC*<sub>2</sub>B<sub>10</sub>, 4,1,6-*MC*<sub>2</sub>B<sub>10</sub>, 4,1,10-*MC*<sub>2</sub>B<sub>10</sub>, and 4,1,12-*MC*<sub>2</sub>B<sub>10</sub>) reveals clear preferences. In all cases a qualitative understanding of these was afforded by simple MO arguments applied to the model heteroarene complexes [(PH<sub>3</sub>)<sub>2</sub>PtC<sub>2</sub>B<sub>4</sub>H<sub>6</sub>]<sup>2-</sup> and [(PH<sub>3</sub>)<sub>2</sub>PtCB<sub>5</sub>H<sub>6</sub>]<sup>3-</sup>. Moreover, DFT calculations on [(PH<sub>3</sub>)<sub>2</sub>PtC<sub>2</sub>B<sub>4</sub>H<sub>6</sub>]<sup>2-</sup> in its various isomeric forms approximately reproduced the observed conformations in the 4,1,2-, 4,1,6-, and 4,1,10-*MC*<sub>2</sub>B<sub>10</sub> species, although analogous calculations on [(PH<sub>3</sub>)<sub>2</sub>PtCB<sub>5</sub>H<sub>6</sub>]<sup>3-</sup> did not reproduce the conformation observed in the 4,1,12-*MC*<sub>2</sub>B<sub>10</sub> metallocarborane. DFT calculations on (PH<sub>3</sub>)<sub>2</sub>PtC<sub>2</sub>B<sub>10</sub>H<sub>12</sub> yielded good agreement with experimental conformations in all four isomeric cases. Apparent discrepancies between observed and computed Pt–C distances were probed by further refinement of the 4,1,2- model to 1,2-(CH<sub>2</sub>)<sub>3</sub>-4,4-(PMe<sub>3</sub>)<sub>2</sub>-4,1,2-*closo*-PtC<sub>2</sub>B<sub>10</sub>H<sub>10</sub>. This still has a more distorted structure than measured experimentally for 1,2-(CH<sub>2</sub>)<sub>3</sub>-4,4-(PMe<sub>2</sub>Ph)<sub>2</sub>-4,1,2-*closo*-PtC<sub>2</sub>B<sub>10</sub>H<sub>10</sub>, but the structural differences lie on a very shallow potential energy surface. For the model compound a hencicosahedral transition state was located 8.3 kcal mol<sup>-1</sup> above the ground-state structure, consistent with the fluxionality of 1,2-(CH<sub>2</sub>)<sub>3</sub>-4,4-(PMe<sub>2</sub>Ph)<sub>2</sub>-4,1,2-*closo*-PtC<sub>2</sub>B<sub>10</sub>H<sub>10</sub> in solution.

### Introduction

There is significant current interest in supracosahedral heteroborane chemistry, an area of study which began more than three decades ago with the synthesis<sup>1</sup> and subsequent structural study<sup>2</sup> of the first such species, the 13-vertex cobaltacarborane 4-Cp-4,1,6-*closo*-CoC<sub>2</sub>B<sub>10</sub>H<sub>12</sub>. For many years large boron-based polyhedra have been of interest to computational chemists<sup>3</sup> and have represented a significant challenge to experimentalists. Although well over a hundred 13-vertex metallocarboranes are now known, there is still only a handful of 14-vertex species<sup>4</sup> and only two 15-vertex species.<sup>5</sup> However, recent advances,<sup>6</sup>

including the synthesis of supraicosahedral carboranes,<sup>7</sup> are laying the foundations for the eventual synthesis of larger and larger heteroboranes to complement the theoretical work.

The usual structure adopted by 13-vertex metallocarboranes is the dicosahedron, **I** (Chart 1). This structure (of idealized C<sub>2v</sub> symmetry) has two degree-six (with respect to the polyhedron) vertices (vertices 4 and 5) and one degree-four vertex (vertex 1); all the remaining vertices are of degree-five. Recently, we have reported a variation of this basic shape.<sup>8</sup> In the

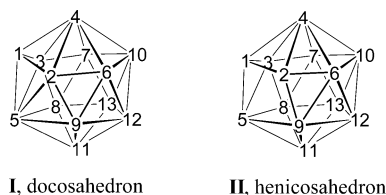
<sup>†</sup> Heriot-Watt University.

<sup>‡</sup> Baylor University.

- (1) Dunks, G. B.; McKown, M. M.; Hawthorne, M. F. *J. Am. Chem. Soc.* **1971**, *93*, 2541.
- (2) Churchill, M. R.; DeBoer, B. G. *J. Chem. Soc., Chem. Commun.* **1972**, 1326.
- (3) (a) Brown, L. D.; Lipscomb, W. N. *Inorg. Chem.* **1977**, *16*, 2989. (b) Bicerano, J.; Marynick, D. S.; Lipscomb, W. N. *Inorg. Chem.* **1978**, *17*, 2041. (c) Bicerano, J.; Marynick, D. S.; Lipscomb, W. N. *Inorg. Chem.* **1978**, *17*, 3443. (d) Lipscomb, W. N.; Massa, L. *Inorg. Chem.* **1992**, *31*, 2297. (e) Schleyer, P. v. R.; Najafian, K.; Mebel, A. M. *Inorg. Chem.* **1998**, *37*, 6765. (f) Balakrishnan, M. M.; Hoffmann, R.; Pancharatna, P. D.; Jemmis, E. D. *Inorg. Chem.* **2003**, *42*, 4650. (g) Wang, Z. X.; Schleyer, P. v. R. *J. Am. Chem. Soc.* **2003**, *125*, 10484.

- (4) (a) Evans, W. J.; Hawthorne, M. F. *J. Chem. Soc., Chem. Commun.* **1974**, 38. (b) Maxwell, W. M.; Bryan, R. F.; Grimes, R. N. *J. Am. Chem. Soc.* **1977**, *99*, 4008. (c) Maxwell, W. M.; Weiss, R.; Sinn, E.; Grimes, R. N. *J. Am. Chem. Soc.* **1977**, *99*, 4016. (d) Pipal, J. R.; Grimes, R. N. *Inorg. Chem.* **1978**, *17*, 6. (e) Ellis, D.; Lopez, M. E.; McIntosh, R.; Rosair, G. M.; Welch, A. J. *J. Chem. Commun.* **2005**, 1917.
- (5) (a) McIntosh, R. D.; Ellis, D.; Rosair, G. M.; Welch, A. J. *Angew. Chem., Int. Ed.* **2006**, *45*, 4313. (b) Deng, L.; Zhang, J.; Chan, H.-S.; Xie, Z. *Angew. Chem., Int. Ed.* **2006**, *45*, 4309.
- (6) For example: (a) Ellis, D.; Lopez, M. E.; McIntosh, R.; Rosair, G. M.; Welch, A. J.; Quenardelle, R. *J. Chem. Commun.* **2005**, 1348. (b) Deng, L.; Chan, H.-S.; Xie, Z. *J. Am. Chem. Soc.* **2006**, *128*, 5219.
- (7) (a) Burke, A.; Ellis, D.; Giles, B. T.; Hodson, B. E.; Macgregor, S. A.; Rosair, G. M.; Welch, A. J. *Angew. Chem., Int. Ed.* **2003**, *42*, 225. (b) Deng, L.; Chan, H.-S.; Xie, Z. *Angew. Chem., Int. Ed.* **2005**, *44*, 2128.
- (8) McIntosh, R.; Ellis, D.; Gil-Lostes, J.; Dalby, K. J.; Rosair, G. M.; Welch, A. J. *Dalton Trans.* **2005**, 1842.

Chart 1

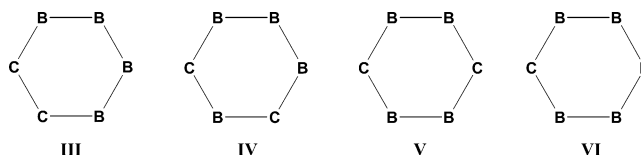


hencicosahedron, **II**, the 2–5 connectivity of the dicosahedron is missing, and the structure (of idealized  $C_s$  symmetry) has a trapezoidal 1295 face.

In all known  $MC_2B_{10}$  13-vertex metallocarboranes the metal atom occupies vertex 4, one of the positions of highest connectivity, and one carbon atom occupies vertex 1, the lowest-connected position, a simple consequence of the relative electronegativities of metals, carbon, and boron. Thus, for  $MC_2B_{10}$  species isomers are possible, based on the location of the second cage C atom. Since 13-vertex metallocarboranes are usually prepared from reduction and subsequent metalation of *closo*- $C_2B_{10}$  carboranes, kinetic isomers of  $MC_2B_{10}$  configuration arise from the use of different carborane isomers: (i) reduction of 1,2-*closo*- $C_2B_{10}$  carborane causes the C atoms to spontaneously separate,<sup>9</sup> affording  $[7,9\text{-nido-}C_2B_{10}]^{2-}$ , and metalation then affords 4,1,6- $MC_2B_{10}$  metallocarboranes;<sup>10</sup> (ii) reduction of 1,7-*closo*- $C_2B_{10}$  carborane also yields  $[7,9\text{-nido-}C_2B_{10}]^{2-}$ ,<sup>11</sup> hence the same 4,1,6- $MC_2B_{10}$  species; (iii) in contrast, reduction of 1,12-*closo*- $C_2B_{10}$  carborane affords  $[7,10\text{-nido-}C_2B_{10}]^{2-}$  and thus 4,1,10- $MC_2B_{10}$  clusters upon metalation.<sup>6a</sup> Thermolysis of these kinetic metallocarborane isomers causes rearrangement to thermodynamically preferred ones; heating 4,1,6- $MC_2B_{10}$  results, for some metals, in progressive conversion to 4,1,8- and then 4,1,12- $MC_2B_{10}$  isomers,<sup>12</sup> and thermolysis of 4,1,10- $MC_2B_{10}$  has been shown to produce the 4,1,12- isomer.<sup>6a</sup> A final known isomer is 4,1,2- $MC_2B_{10}$ . This form is afforded either by direct insertion of a highly nucleophilic metal fragment into a 1,2-*closo*- $C_2B_{10}$  cage<sup>13</sup> or by reduction and then metalation of a C,C-tethered 1,2- $C_2B_{10}$  species.<sup>8</sup>

Focusing only on the metal coordination sphere we therefore now have access to four types of supracosahedral  $MC_2B_{10}$  metallocarboranes. In three of these the metal fragment is bonded to  $C_2B_4$  ligand faces with the cage C atoms either adjacent, **III**

Chart 2



(the isomer 4,1,2- $MC_2B_{10}$ ); separated by a single B atom, **IV** (the isomer 4,1,6- $MC_2B_{10}$ ); or separated by two B atoms, **V** (the isomer 4,1,10- $MC_2B_{10}$ ) (see Chart 2). In the fourth type of  $MC_2B_{10}$  metallocarborane the metal is bound to a  $CB_5$  ligand face, **VI** (the isomers 4,1,8- or 4,1,12- $MC_2B_{10}$ ).

Several years ago one of us was involved with studies into the conformational preferences and slipping distortions of  $\{ML_2\}$  fragments ( $M$  = group 10 metal;  $L$  = 2e ligand, e.g.,  $PR_3$ ) with respect to five-atom carborane ligand faces ( $C_2B_3$  faces with both adjacent and nonadjacent C atoms, and the  $CB_4$  face) in icosahedral metallocarboranes.<sup>14</sup> In the present paper we describe, by a joint experimental and computational study, the ways in which  $\{ML_2\}$  fragments now bond to the four different types of six-atom carborane faces (**III**–**VI** above) in supracosahedral metallocarboranes, extending and complementing the earlier work.

## Experimental Section

**Synthesis: General.** Experiments were performed under dry, oxygen-free  $N_2$  using standard Schlenk techniques, with some subsequent manipulation in the open laboratory. Solvents were freshly distilled over  $CaH_2$  ( $CH_2Cl_2$ ) or Na wire (THF, 40–60 petroleum ether) or stored over 4 Å molecular sieves ( $CDCl_3$ ,  $CD_2Cl_2$ ) and were degassed ( $3 \times$  freeze–pump–thaw cycles) before use. Preparative thin layer chromatography (TLC) employed 20 cm  $\times$  20 cm Kieselgel 60  $F_{254}$  glass plates. For compounds **3** and **6** IR spectra were recorded from  $CH_2Cl_2$  solutions using a Perkin-Elmer Spectrum RX FT spectrophotometer, and  $^1H$  NMR spectra were recorded at 200.1 MHz (Bruker AC200 spectrometer) and  $^{31}P$  and  $^{11}B$  spectra at 162.0 and 128.4 MHz, respectively (Bruker DPX400 spectrometer) from  $CDCl_3$  solutions at room temperature (Heriot-Watt University). For compound **8** IR spectra were recorded from  $CH_2Cl_2$  solutions using a Bruker IFS25 FT spectrophotometer, and NMR spectra were recorded from  $CD_2Cl_2$  solutions using a Bruker AMX360 spectrometer at 360.1, 115.5, and 90.6 MHz for  $^1H$ ,  $^{11}B$ , and  $^{13}C$ , respectively (Baylor University). Elemental analyses were determined by the appropriate departmental or commercial services. The starting materials 1,2-( $CH_2$ )<sub>3</sub>-1,2-*closo*- $C_2B_{10}H_{10}$ ,<sup>15</sup>  $[codRhCl]_2$ ,<sup>16</sup> and  $(PMe_2Ph)_2PtCl_2$ <sup>17</sup> were prepared by literature methods or slight variations thereof. All other reagents and solvents were supplied commercially and used as received.

**4,4-( $PMe_2Ph$ )<sub>2</sub>-4,1,6-*closo*-Pt $C_2B_{10}H_{12}$ .** 1,2-*closo*- $C_2B_{10}H_{12}$  (0.045 g, 0.31 mmol) and freshly cut sodium (0.015 g, 0.68 mmol) were stirred in THF (~20 mL) for 18 h. The resulting solution of  $Na_2[C_2B_{10}H_{12}]$  was separated from excess sodium by cannula into a cooled (0 °C) suspension of  $(PMe_2Ph)_2PtCl_2$  (0.15 g, 0.31 mmol) in THF (~20 mL). The reactants were allowed to warm to room temperature and stirred for 18 h. Volatiles were removed in vacuo, leaving a yellow solid which was subsequently dissolved in  $CH_2Cl_2$  (20 mL), filtered, and concentrated. Preparative TLC eluting with  $CH_2Cl_2/40$ –60 petroleum ether (1:1) afforded, as major product, a pale-yellow band ( $R_f$  = 0.15) subsequently shown to be 4,4-( $PMe_2Ph$ )<sub>2</sub>-4,1,6-*closo*-Pt $C_2B_{10}H_{12}$ , com-

- (9) (a) Getman, T. D.; Knobler, C. B.; Hawthorne, M. F. *Inorg. Chem.* **1990**, *29*, 158. (b) McKee, M. L.; Bühl, M.; Schleyer, P. v. R. *Inorg. Chem.* **1993**, *32*, 1712. (c) Hermansson, K.; Wójcik, M.; Sjöberg, S. *Inorg. Chem.* **1999**, *38*, 6039.
- (10) Representative examples: (a) Hewes, J. D.; Knobler, C. B.; Hawthorne, M. F. *J. Chem. Soc., Chem. Commun.* **1981**, 206. (b) Khattar, R.; Knobler, C. B.; Hawthorne, M. F. *J. Am. Chem. Soc.* **1990**, *112*, 4962. (c) Khattar, R.; Knobler, C. B.; Hawthorne, M. F. *Inorg. Chem.* **1990**, *29*, 2191. (d) Khattar, R.; Knobler, C. B.; Johnson, S. E.; Hawthorne, M. F. *Inorg. Chem.* **1991**, *30*, 1970. (e) Khattar, R.; Manning, M. J.; Knobler, C. B.; Johnson, S. E.; Hawthorne, M. F. *Inorg. Chem.* **1992**, *31*, 268. (f) Carr, N.; Mullica, D. F.; Sappenfield, E. L.; Stone, F. G. A.; Went, M. J. *Organometallics* **1993**, *12*, 4350. (g) Li, S.; Mullica, D. F.; Sappenfield, E. L.; Stone, F. G. A. *J. Organometal. Chem.* **1994**, *467*, 95. (h) Mullica, D. F.; Sappenfield, E. L.; Stone, F. G. A.; Woollam, S. F. *Can. J. Chem.* **1995**, *73*, 909. (i) Chui, K.; Yang, Q.; Mak, T. C. W.; Xie, Z. *Organometallics* **2000**, *19*, 1391. (j) Wilson, N. M. M.; Ellis, D.; Boyd, A. S. F.; Giles, B. T.; Macgregor, S. A.; Rosair, G. M.; Welch, A. J. *Chem. Commun.* **2002**, 464. (k) Burke, A.; Ellis, D.; Ferrer, D.; Ormsby, D. L.; Rosair, G. M.; Welch, A. J. *Dalton Trans.* **2005**, 1716.
- (11) Dunks, G. B.; Wiersema, R. J.; Hawthorne, M. F. *J. Am. Chem. Soc.* **1973**, *95*, 3174.
- (12) (a) Dustin, D. F.; Dunks, G. B.; Hawthorne, M. F. *J. Am. Chem. Soc.* **1973**, *95*, 1109. (b) Burke, A.; McIntosh, R.; Ellis, D.; Rosair, G. M.; Welch, A. J. *Collect. Czech. Chem. Commun.* **2002**, *67*, 991.
- (13) Barker, G. K.; Garcia, M. P.; Green, M.; Stone, F. G. A.; Welch, A. J. *J. Chem. Soc., Chem. Commun.* **1983**, 137.

- (14) (a) Mingos, D. M. P.; Forsyth, M. I.; Welch, A. J. *J. Chem. Soc., Chem. Commun.* **1977**, 605. (b) Mingos, D. M. P.; Forsyth, M. I.; Welch, A. J. *J. Chem. Soc., Dalton Trans.* **1978**, 1363.
- (15) Paxon, T. E.; Kaloustian, M. K.; Tom, G. M.; Wiersema, R. J.; Hawthorne, M. F. *J. Am. Chem. Soc.* **1972**, *94*, 4882.
- (16) Chatt, J.; Venanzi, L. M. *J. Chem. Soc.* **1957**, 4735.
- (17) Jenkins, J. M.; Shaw, B. L. *J. Chem. Soc. (A)* **1966**, 770.

pound **3**, (0.38 g, 20%).  $C_{18}H_{34}B_{10}P_2Pt$  requires C 35.1, H 5.58. Found: C 35.2, H 5.60. IR,  $\nu_{max}$  at  $2500\text{ cm}^{-1}$  (B–H).  $^{11}B\{^1H\}$  NMR:  $\delta$  –0.98 (2B), –2.60 (1B), –4.54 (3B), –9.46 (1B), –13.85 (2B), and –15.00 ( $\delta(^{11}B)$ ) = –11.62.  $^1H$  NMR,  $\delta$  7.45–7.25 (m, 10H,  $C_6H_5$ ), 3.95 (br s, 2H,  $C_{cage}H$ ), and 1.7–1.3 (br m, 12H,  $P(CH_3)_2$ ).  $^{31}P\{^1H\}$  NMR:  $\delta$  –17.61 (s,  $J_{PP}$  3894 Hz) and –20.82 (s,  $J_{PP}$  2800 Hz).

**4,4-(PMe<sub>2</sub>Ph)<sub>2</sub>-4,1,10-closo-PtC<sub>2</sub>B<sub>10</sub>H<sub>12</sub>**. 1,12-closo-C<sub>2</sub>B<sub>10</sub>H<sub>12</sub> (0.10 g, 0.69 mmol) was cooled to –80 °C. Ammonia (~20 mL) and freshly cut sodium (0.13 g, 5.6 mmol) were added, and the resulting dark-blue solution was stirred for 2 h. Following removal of the ammonia in vacuo the residue was extracted into THF (20 mL) and transferred, by cannula, to a frozen solution of (PMe<sub>2</sub>Ph)<sub>2</sub>PtCl<sub>2</sub> (0.37 g, 0.69 mmol) in THF (20 mL). The reaction mix was allowed to warm to room temperature and stirred for 30 min (**warning – prolonged stirring leads to significant decomposition!**). Volatiles were removed in vacuo, and the yellow residue was extracted into CH<sub>2</sub>Cl<sub>2</sub> (20 mL), filtered, and then purified by preparative TLC eluting with CH<sub>2</sub>Cl<sub>2</sub>/40–60 petroleum ether (7:3) to afford, as a narrow yellow band ( $R_f$  = 0.29), the compound 4,4-(PMe<sub>2</sub>Ph)<sub>2</sub>-4,1,10-closo-PtC<sub>2</sub>B<sub>10</sub>H<sub>12</sub>, compound **6**, (0.02 g, 10%). IR,  $\nu_{max}$  at  $2529\text{ cm}^{-1}$  (B–H).  $^{11}B\{^1H\}$  NMR:  $\delta$  15.91 (2B), 11.04 (1B), 0.17 (1B), –8.38 (2B), –16.30 (2B) and –22.83 (2B),  $\langle\delta(^{11}B)\rangle$  = 0.36.  $^1H$  NMR:  $\delta$  7.6–7.1 (m, 10H,  $C_6H_5$ ), 4.3 (br s, 1H,  $C_{cage}H$ ), 2.7 (br s, 1H,  $C_{cage}H$ ) and 1.9–1.2 (br m, 12H,  $P(CH_3)_2$ ).  $^{31}P\{^1H\}$  NMR:  $\delta$  –13.16 (s,  $J_{PP}$  3013 Hz).

**[N(PPh<sub>3</sub>)<sub>2</sub>][4,4-cod-4,1,10-closo-RhC<sub>2</sub>B<sub>10</sub>H<sub>12</sub>]**. Similarly, from 1,12-closo-C<sub>2</sub>B<sub>10</sub>H<sub>10</sub> (0.20 g, 1.39 mmol) and [codRhCl]<sub>2</sub> (0.34 g, 0.69 mmol), followed by metathesis with [N(PPh<sub>3</sub>)<sub>2</sub>]Cl (0.80 g, 1.39 mmol) was isolated yellow [N(PPh<sub>3</sub>)<sub>2</sub>][4,4-cod-4,1,10-closo-RhC<sub>2</sub>B<sub>10</sub>H<sub>12</sub>], salt **8**, (0.50 g, 40%) as the major mobile product following column chromatography (eluting with CH<sub>2</sub>Cl<sub>2</sub>/40–60 petroleum ether, 7:3).  $C_{46}H_{54}B_{10}NP_2Rh$  requires C 61.8, H 6.1, N 1.6. Found: C 62.0, H 6.2, N 1.7. IR:  $\nu_{max}$  at  $2531\text{ cm}^{-1}$  (B–H).  $^{11}B\{^1H\}$  NMR ( $CD_2Cl_2$ )  $\delta$  –4.5 (2B), –6.0 (2B), –12.3 (1B), –13.5 (1B), –16.2 (2B) and –17.2 (2B),  $\langle\delta(^{11}B)\rangle$  = –11.4.  $^1H$  NMR ( $CD_2Cl_2$ ):  $\delta$  7.8–7.5 (m, 30H,  $C_6H_5$ ), 5.06 (vbr, 1H,  $C_{cage}H$ ), 4.35 (br, 4H, =CH), 2.22 (br, 8H,  $CH_2$ ), and 2.05 (vbr, 1H,  $C_{cage}H$ ).  $^{13}C\{^1H\}$  NMR ( $CD_2Cl_2$ ): 133.8–126.5 ( $C_6H_5$ ), 79.0 (br,  $C_{cage}$ ), 77.1 [d,  $J(RhC)$  10 Hz, =CH], 42.4 (br,  $C_{cage}$ ) and 32.2 ( $CH_2$ ).

**Crystallography.** Intensity data were collected on single crystals of **3**, **6**, and **8**·1/2CH<sub>2</sub>Cl<sub>2</sub> on a Bruker X8 APEX2 diffractometer,<sup>18</sup> with crystals mounted in inert oil on a glass fiber and cooled to 100 K (**3** and **6**, Heriot-Watt University) or 110 K (**8**, Baylor University) by an Oxford Cryosystems Cryostream. The structures were solved by direct methods and refined by full-matrix least-squares.<sup>19</sup> All non-H atoms were refined with anisotropic displacement parameters. In compound **6** the cage is disordered about a crystallographic  $C_2$  axis, and the disorder was modeled by two intersecting half-occupancy pentagonal pyramids for the lower cage belt (B5B9B12B13B8B11), co-incident at the (crystallographically equivalent) B8 and B9 positions. In spite of this disorder C1 ( $\equiv$  C10) was unambiguously identified as a carbon atom. For **3** and **8** cage-bound H atoms were located in difference Fourier maps and freely refined, but with thermal parameters set to  $1.2 \times U_{eq}$  of the attached B or C atom. In the case of **6**, some cage BH atoms were located and positionally refined, but restrained to B–H 1.10(2) Å, while others were set in calculated positions; the position of the single CH was also calculated, with C–H 1.10 Å; again, thermal parameters for all cage H atoms were set to  $1.2 \times U_{eq}$  of the attached B or C atom. Note that, although B11 is disordered over two positions, its attached H atom sits on the crystallographic  $C_2$  axis. In **3** and **6**, methyl H atoms (C–H 0.98 Å) and phenyl H atoms (C–H 0.95 Å) were placed in calculated but riding positions, with  $U_H$  set to 1.5 or  $1.2 \times U_{eq}$ , respectively. For **8**, non-cage H atoms were set in calculated,

**Table 1.** Crystallographic Data

	<b>3</b>	<b>6</b>	<b>8</b> ·1/2CH <sub>2</sub> Cl <sub>2</sub>
formula	$C_{18}H_{34}B_{10}P_2Pt$	$C_{18}H_{34}B_{10}P_2Pt$	$C_{46.5}H_{55}B_{10}ClNP_2Rh$
$M_r$	615.58	615.58	936.22
system	monoclinic	monoclinic	triclinic
space group	$P2_1/c$	$C2/c$	$P$
$a/\text{Å}$	13.6694(9)	20.335(3)	10.056(5)
$b/\text{Å}$	10.5522(7)	10.4382(14)	14.692(7)
$c/\text{Å}$	17.3895(12)	13.5990(19)	17.296(13)
$\alpha/\text{deg}$	90	90	113.67(4)
$\beta/\text{deg}$	100.028(3)	122.496(3)	100.35(4)
$\gamma/\text{deg}$	90	90	98.26(3)
$V/\text{Å}^3$	2470.0(3)	2434.6(6)	2235(2)
$Z$	4	4	2
$D_c/Mg\text{ m}^{-3}$	1.655	1.679	1.391
$\mu/\text{mm}^{-1}$	5.816	5.901	0.550
$F(000)$	1200	1200	966
$\theta_{max}$	33.22	36.29	27.64
data measured	34349	63206	45526
unique data, $n$	9430	5859	10159
$R_{int}$	0.0229	0.0464	0.0664
max, min. tfs	0.498, 0.315	0.702, 0.566	0.921, 0.803
$R1^a$	0.0182	0.0378	0.0601
wR2 <sup>a</sup>	0.0397	0.0523	0.1199
$S^a$	1.184	0.923	0.998
variables, $p$	320	169	596
$\Delta\rho_{max}, \Delta\rho_{min}/e\text{ Å}^{-3}$	2.087, –1.294	3.261, –1.891	1.801, –1.745

<sup>a</sup>  $R1 = \sum(|F_o| - |F_c|)/\sum|F_o|$ ,  $wR2 = [\sum[w(F_o^2 - F_c^2)^2]/\sum w(F_o^2)^2]^{1/2}$ ,  $S = [\sum[w(F_o^2 - F_c^2)^2/(n - p)]]^{1/2}$ , where  $n$  is the number of data and  $p$  the number of parameters.  $R1$  and  $wR2$  quoted for *all* data.

riding positions, with C–H 0.95 (phenyl), 0.99 ( $CH_2$ ) or 1.00 (cod-CH) Å, and  $U_H$  set to  $1.2 \times U_{eq}$ . The  $CH_2Cl_2$  of solvation of **8** is disordered about an inversion center and was refined with C–Cl restrained to 1.76(2) Å. Table 1 contains further experimental details.

**Calculations.** All geometries were optimized at the B3LYP<sup>20</sup> level with the basis set for all atoms of double- $\zeta$  quality. For carbon, hydrogen, and boron Pople's 6-31G(d,p) basis set was used, while for platinum and phosphorus the Stuttgart relativistic ECP<sup>21</sup> was employed with an additional d-polarization function on phosphorus.<sup>22</sup> Frequency calculations were performed to determine the nature of the optimized geometries. The Gaussian 03 program<sup>23</sup> was used for all calculations. Optimized geometries are displayed via Mercury.<sup>24</sup>

## Results and Discussion

This paper is concerned with the conformations of nine 13-vertex metallocarboranes, compounds **1–9**. Six of these compounds (**1**, **2**, **4**, **5**, **7**, and **9**) have already been described in the literature (although their conformations were not discussed), and three (**3**, **6** and **8**) are new. The compounds are summarized in Table 2 and sketched in Chart 3.

**1. Synthesis and Characterization. 4,1,2-MC<sub>2</sub>B<sub>10</sub> Compounds.** The synthesis, spectroscopic characterization, and structural studies of the platina- and nickelacarboranes 1,2-( $CH_2$ )<sub>3</sub>-4,4-(PMe<sub>2</sub>Ph)<sub>2</sub>-4,1,2-closo-PtC<sub>2</sub>B<sub>10</sub>H<sub>10</sub>, **1**, and 1,2-( $CH_2$ )<sub>3</sub>-4,4-dppe-4,1,2-closo-NiC<sub>2</sub>B<sub>10</sub>H<sub>10</sub>, **2**, (dppe = Ph<sub>2</sub>PCH<sub>2</sub>CH<sub>2</sub>PPh<sub>2</sub>)

(18) Bruker AXS APEX2, version 1.0-8; Bruker AXS Inc.: Madison, WI, U.S.A., 2003.

(19) Sheldrick, G. M. *SHELXTL*, versions 5.1 and 6.12; Bruker AXS Inc.: Madison, WI, U.S.A., 1999 and 2001, respectively.

(20) (a) Becke, A. D. *J. Chem. Phys.* **1993**, *98*, 1372. (b) Becke, A. D. *J. Chem. Phys.* **1993**, *98*, 5648. (c) Lee, C.; Yang, W.; Parr, R. G. *Phys. Rev. B* **1988**, *37*, 785. (d) Becke, A. D. *Phys. Rev. A* **1988**, *38*, 3098.

(21) (a) Bergner, A.; Dolg, M.; Kuechle, H.; Stoll, H.; Preuss, H. *Mol. Phys.* **1993**, *80*, 1431. (b) Kaupp, M.; Schleyer, P. v. R.; Stoll, H.; Preuss, H. *J. Chem. Phys.* **1991**, *94*, 1360. (c) Dolg, M.; Stoll, H.; Preuss, H.; Pitzer, R. M. *J. Phys. Chem.* **1993**, *97*, 5852.

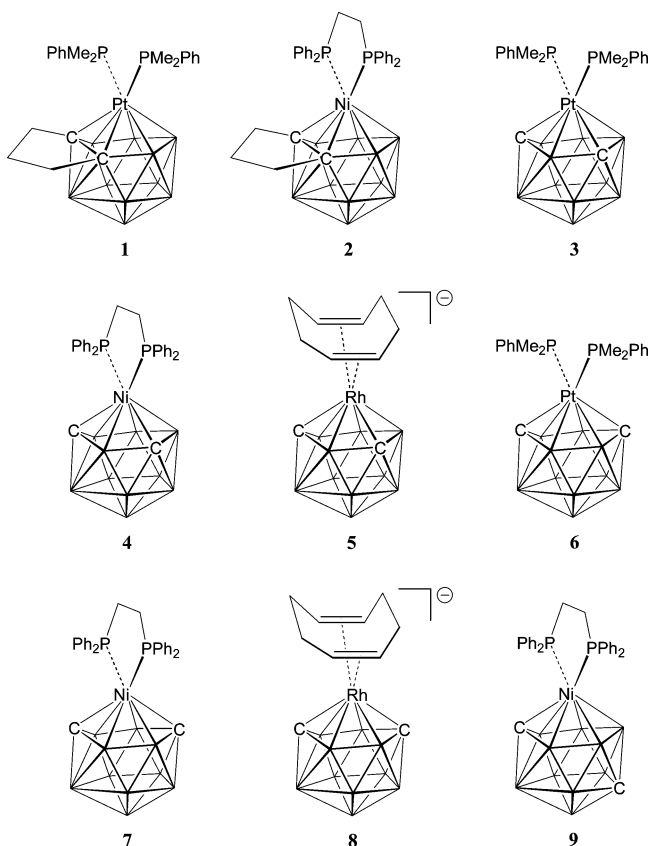
(22) Höllwarth, A.; Böhme, M.; Dapprich, S.; Ehlers, A. W.; Gobbi, A.; Jonas, V.; Köhler, K. F.; Stegmann, R.; Veldkamp, A.; Frenking, G. *Chem. Phys. Lett.* **1993**, *208*, 237.

(23) Frisch, M. J., et al. *Gaussian 03, revision C.02*; Gaussian Inc., Wallingford, CT, U.S.A., 2004.

(24) Mercury, version 1.4.1; Cambridge Crystallographic Data Center: Cambridge, UK, 2006.

**Table 2.** Summary of Compounds Described

	4,1,2- $[MC_2B_{10}]$ (ligand type III)	4,1,6- $[MC_2B_{10}]$ (ligand type IV)	4,1,10- $[MC_2B_{10}]$ (ligand type V)	4,1,12- $[MC_2B_{10}]$ (ligand type VI)
$[M] = P_2Pt^a$	<b>1</b>	<b>3</b>	<b>6</b>	
$[M] = dppeNi$	<b>2</b>	<b>4</b>	<b>7</b>	<b>9</b>
$[M]^- = codRh$		<b>5</b>	<b>8</b>	

<sup>a</sup> P =  $PMe_2Ph$ **Chart 3**

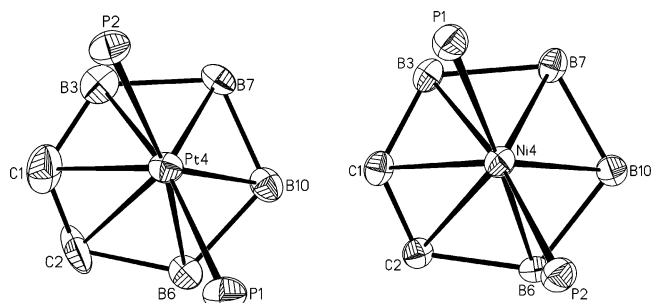
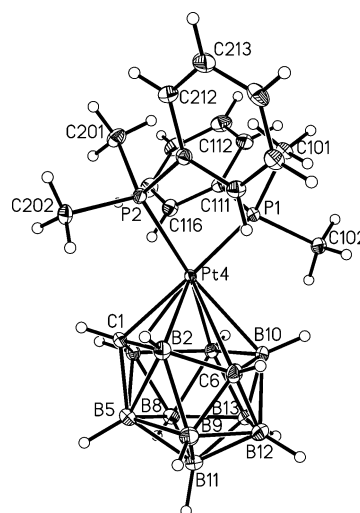
Unlabeled cage vertices are BH  
 Except for **1** and **2** cage C vertices are CH

were described recently.<sup>8</sup> The cages in both these metallacarboranes are dicosahedral with formal connectivities between C2 and B5, although that for **1** is relatively long, 2.055(12) Å, consistent with a distortion toward a hencicosahedral cage.

Figure 1 shows views of the central  $ML_2C_2B_4$  portions of **1** and **2**, illustrating the conformations of the  $\{ML_2\}$  fragments relative to the  $C_2B_4$  ligand face. A convenient (arbitrary) quantitative measure of these conformations is  $\theta$ , the dihedral angle between  $ML_2$  and  $MC1B10B11$  (compounds **1–5**, **9**) or  $MC1C10B11$  (compounds **6–8**) planes, where  $0 < \theta < 90^\circ$  represents, in projection, one ligand  $L$  lying in the B3 quadrant, and  $90 < \theta < 180^\circ$  represents  $L$  in the B7 quadrant. For compounds **1** and **2**  $\theta$  is  $61.1^\circ$  and  $64.6^\circ$ , respectively.

All attempts to prepare  $[1,2-(CH_2)_3-4,4-cod-4,1,2-closo-RhC_2B_{10}H_{10}]^-$ , the rhodacarborane anion analogue of **1** and **2**, were unsuccessful.

**4,1,6- $MC_2B_{10}$  Compounds.** We have prepared the platinum complex 4,4-( $PMe_2Ph$ )<sub>2</sub>-4,1,6-*closo*- $PtC_2B_{10}H_{12}$ , **3**, to complement its previously described analogues, namely the nickelacarborane 4,4-dppe-4,1,6-*closo*- $NiC_2B_{10}H_{12}$ , **4**,<sup>25</sup> and the rho-

**Figure 1.** Experimental conformations of the  $\{MP_2\}$  fragments in (left) **1** ( $\theta = 61.1^\circ$ ) and (right) **2** ( $\theta = 64.6^\circ$ ).**Figure 2.** Perspective view of compound **3**. Thermal ellipsoids are drawn at the 50% probability level, except for H atoms which have an artificial radius for clarity.

dacarborane salt  $[N(PPh_3)_2][4,4-cod-4,1,6-closo-RhC_2B_{10}H_{12}]$ , **5**.<sup>26</sup> Sodium reduction of 1,2-*closo*-1,2- $C_2B_{10}H_{12}$  followed by treatment with  $(PMe_2Ph)_2PtCl_2$  and workup involving TLC affords the yellow compound **3** in reasonable yield. The  $^{11}B\{^1H\}$  NMR spectrum of **3** reveals six resonances between  $\delta$  0 and  $-15$ , with relative integrals 2:1:3[2+1 co-incidence]:1:2:1 (from high frequency to low frequency) and with a weighted average  $^{11}B$  chemical shift,  $\langle\delta(^{11}B)\rangle$ , of  $-11.6$ . In the  $^1H$  NMR spectrum is a single resonance for cage CH atoms,  $\delta$  3.95, whereas the  $^{31}P\{^1H\}$  NMR spectrum reveals two singlets (with attendant  $^{195}Pt$  satellites) at  $\delta$   $-17.6$  and  $-20.8$ . All these data are consistent with a (time-averaged) structure in solution of  $C_s$  symmetry, with the  $PtP_2$  plane lying on the molecular mirror plane.

Compound **3** was further characterized by a crystallographic study. Figure 2 contains a perspective view of the compound, and Table 3 lists selected molecular parameters. The cage of **3**, like that of **4** and **5**, is a dicosahedron, but is considerably distorted by, in particular, a very long  $Pt4\cdots C6$  distance, 2.813(13) Å. Note that the  $Pt4-C6$  vector, in projection (see Figure 3, left) lies effectively perpendicular to the  $PtP_2$  plane. B–B distances within **3** follow the trends already established<sup>10k,25</sup> for 4,1,6- $MC_2B_{10}$  polyhedra, with connectivities involving the degree-six B atom B5 being relatively long, particularly so if

(25) Laguna, M. A.; Ellis, D.; Rosair, G. M.; Welch, A. J. *Inorg. Chim. Acta* **2003**, *347*, 161.

(26) Hodson, B. E.; McGrath, T. D.; Stone, F. G. A. *Organometallics* **2005**, *24*, 1638.

**Table 3.** Selected Molecular Parameters (Å, deg) in 4,4-(PMe<sub>2</sub>Ph)<sub>2</sub>-4,1,6-*closo*-PtC<sub>2</sub>B<sub>10</sub>H<sub>12</sub>, **3**

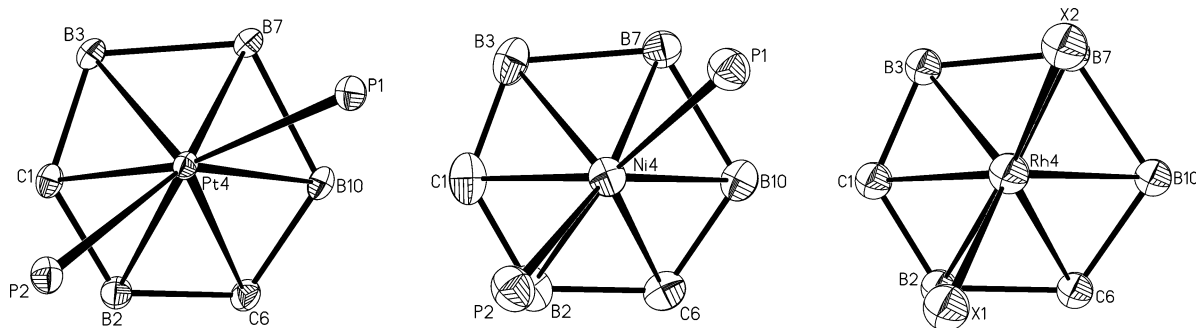
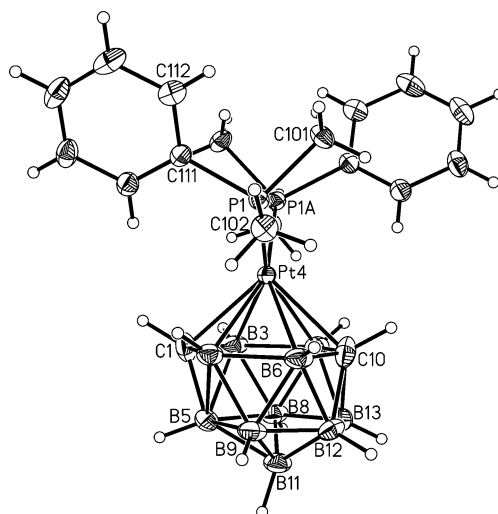
C1–B2	1.555(2)	Pt4···C6	2.8131(13)	B8–B11	1.766(2)
C1–B3	1.573(2)	Pt4–B7	2.2631(14)	B8–B13	1.758(2)
C1–Pt4	2.1652(12)	Pt4–B10	2.3692(14)	B9–B11	1.730(3)
C1–B5	1.742(2)	B5–B8	1.867(2)	B9–B12	1.750(2)
B2–Pt4	2.4438(15)	B5–B9	1.957(3)	B10–B12	1.827(2)
B2–B5	2.259(3)	B5–B11	1.804(2)	B10–B13	1.816(2)
B2–C6	1.623(2)	C6–B9	1.662(2)	B11–B12	1.785(2)
B2–B9	1.932(2)	C6–B10	1.693(2)	B11–B13	1.802(2)
B3–Pt4	2.3961(14)	C6–B12	1.647(2)	B12–B13	1.768(3)
B3–B5	1.884(2)	B7–B8	1.783(2)	Pt4–P1	2.2710(3)
B3–B7	1.856(2)	B7–B10	1.862(2)	Pt4–P2	2.3129(4)
B3–B8	1.752(2)	B7–B13	1.764(2)	P1–Pt4–P2	92.363(14)

the other B atom is also connected to the degree-six Pt atom and one or more cage C atoms. Thus, B2–B5, 2.259(3) Å, is the longest, followed by B9–B5, 1.957(3) Å, B3–B5, 1.884(2) Å, and B8–B5, 1.867(2) Å. In **3** the conformation of the PtP<sub>2</sub> plane is defined by  $\theta = 148.7^\circ$ .

The C<sub>s</sub> symmetry of the cage of **3** implied by the NMR data can be readily understood in terms of the double diamond–square–diamond fluxional process first suggested by Hawthorne for the CpCo system<sup>12a</sup> and recently confirmed computationally by us for the Sn<sup>10j</sup> and ( $\eta$ -C<sub>6</sub>H<sub>6</sub>)Ru<sup>10k</sup> systems. This process effectively generates a mirror plane through atoms Pt4, B2, B11, and B7 (the integral-1 B atoms), which relates pairwise B3 and B10, B5 and B9, and B8 and B12 (the integral-2 B atoms) and renders equivalent the two cage C atoms. To maintain the inequivalence of the P atoms all that is required is a synchronous libration of the PtP<sub>2</sub> unit about the Pt4B2B7 plane (see Figure 3). Full rotation of the {PtP<sub>2</sub>} fragment, which would render the P atoms equivalent, presumably occurs at higher temperatures, but this was not explored as attempts to isomerize **3** by thermolysis (see later) led only to decomposition.

Compound **4** crystallizes (as its 1:1 CH<sub>2</sub>Cl<sub>2</sub> solvate) in two crystalline modifications, **4** $\alpha$  and **4** $\beta$ , but the cages of the two forms are practically superimposable. The angle  $\theta$ , defined as above, is 134.6° for **4** $\alpha$  and 136.7° for **4** $\beta$ . Figure 3 (left and center) shows views of the MP<sub>2</sub>C<sub>2</sub>B<sub>4</sub> cores of **3** and **4** $\alpha$ , comparing the orientation of the MP<sub>2</sub> planes relative to the carborane ligand faces. To describe the conformation of the {codRh} fragment in the anion of **5** we define X1 and X2 as the midpoints of the cod C=C bonds. Figure 3 (right) is a view of the RhX<sub>2</sub>C<sub>2</sub>B<sub>4</sub> central part of the anion of **5**, and  $\theta$ , the dihedral angle between the RhX<sub>2</sub> and RhC1B10B11 planes, is 115.1°.

**4,1,10-MC<sub>2</sub>B<sub>10</sub> Compounds.** The nickelacarborane 4,4-(dppe)-4,1,10-*closo*-NiC<sub>2</sub>B<sub>10</sub>H<sub>12</sub>, **7**, afforded by nickelation of reduced 1,12-*closo*-C<sub>2</sub>B<sub>10</sub>H<sub>12</sub>, has been reported in a recent

**Figure 3.** Experimental conformations of the {ML<sub>2</sub>} fragments in **3** (left;  $\theta = 148.7^\circ$ ), **4** $\alpha$  (center;  $\theta = 134.6^\circ$ ) and **5** (right;  $\theta = 115.1^\circ$ ).**Figure 4.** Perspective view of compound **6** showing, for clarity, only one of the disordered pentagonal pyramids used to model the lower part of the molecule. Thermal ellipsoids as for Figure 2. Note that the polyhedral numbering in this Figure is conventional and not necessarily that in the corresponding CIF.

communication.<sup>6a</sup> Similar treatment of the [7,10-*nido*-C<sub>2</sub>B<sub>10</sub>H<sub>12</sub>]<sup>2-</sup> anion with (PMe<sub>2</sub>Ph)<sub>2</sub>PtCl<sub>2</sub> or with [codRhCl]<sub>2</sub> (the latter followed by cation metathesis) yields the yellow platina- and rhodacarborane species 4,4-(PMe<sub>2</sub>Ph)<sub>2</sub>-4,1,10-*closo*-PtC<sub>2</sub>B<sub>10</sub>H<sub>12</sub>, **6**, and [N(PPh<sub>3</sub>)<sub>2</sub>][4,4-cod-4,1,10-*closo*-RhC<sub>2</sub>B<sub>10</sub>H<sub>12</sub>], **8**, following chromatographic workup. The isolated yield of **6** is relatively poor, but the compound is comparatively unstable. The yield of **8** is reasonable, and certainly **8** is the major reaction product.

NMR spectra of **6** are fully consistent with a C<sub>s</sub> symmetric compound. In the <sup>11</sup>B{<sup>1</sup>H} spectrum are six resonances, 2:1:1:2:2:2 (high to low frequency), between  $\delta +16$  and  $-23$ , with  $\langle\delta(^{11}\text{B})\rangle = 0.4$ , and the <sup>31</sup>P{<sup>1</sup>H} spectrum yields a singlet (with attendant <sup>195</sup>Pt satellites) at  $\delta -13.6$ . There are two cage CH resonances in the <sup>1</sup>H spectrum, at  $\delta 4.3$  and 2.7, implying that these lie on the mirror plane and not across it. A crystallographic study of **6** is fully consistent with these conclusions, but unfortunately suffers from partial disorder of the lower {B<sub>6</sub>H<sub>6</sub>} fragment, which has been modeled as two interpenetrating pentagonal pyramids (see Experimental Section). Figure 4 is a perspective view of one molecule of **6** in which only one of these lower pentagonal pyramids is shown. Table 4 lists key molecular parameters. Crystallographically, the disordered model has precise C<sub>2</sub> symmetry, but (both) the disordered components also have effective C<sub>s</sub> symmetry, at least as far as the P<sub>2</sub>PtC<sub>2</sub>B<sub>10</sub> fragments are concerned. Although the disorder is also manifest in the upper C<sub>2</sub>B<sub>4</sub> portion of the carborane ligand

**Table 4.** Selected Molecular Parameters (Å, deg) in 4,4-(PMe<sub>2</sub>Ph)<sub>2</sub>-4,1,10-*closo*-PtC<sub>2</sub>B<sub>10</sub>H<sub>12</sub>, **6**

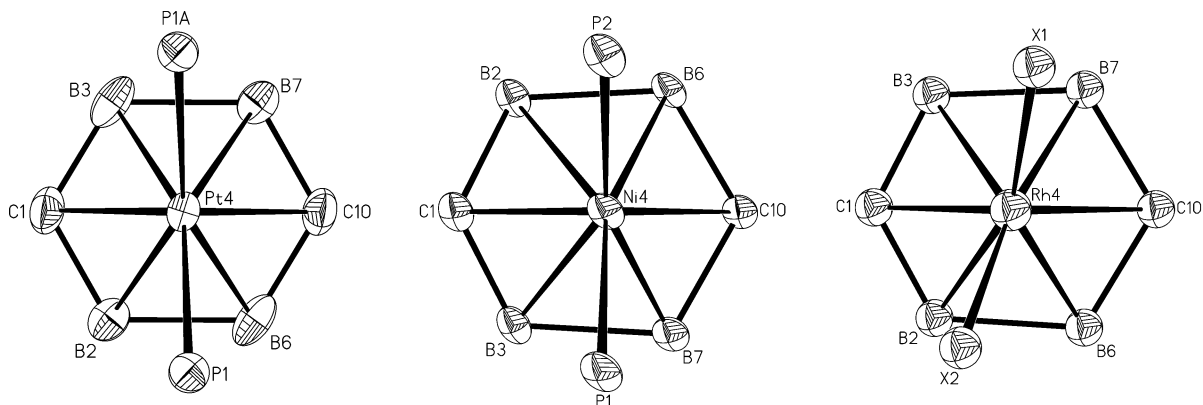
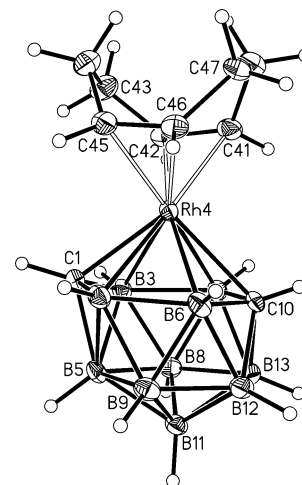
C1–B2	1.599(3)	B3–B5	2.117(6)	B8–B13	1.714(6)
C1–B3	1.611(4)	B3–B8	1.781(3)	B9–B12	1.666(6)
C1–Pt4	2.357(2)	B5–B8	1.983(7)	C10–B12	1.815(5)
C1–B5	1.635(6)	B5–B9	1.881(6)	C10–B13	1.747(5)
B2–Pt4	2.337(2)	B5–B11	1.777(7)	B11–B12	1.762(7)
B2–B5	2.055(5)	B6–B12	1.694(5)	B11–B13	1.762(9)
B2–B6	1.853(4)	B7–B13	1.750(5)	B12–B13	1.751(7)
B2–B9	1.801(3)	B8–B11	1.783(7)	Pt4–P1	2.2937(5)
				P1–Pt4–P1A	91.87(2)

in that the formally degree-four and degree-five atoms C1 and C10 are crystallographically equivalent, the disorder does not influence the broad conclusion regarding the conformation of the PtP<sub>2</sub> unit with respect to the C<sub>2</sub>B<sub>4</sub> ligand face (Figure 5 left).  $\theta$  for **6** is 87.7°. Detailed analysis of the structure of **6** is not warranted because of the crystallographic disorder, save to note very long B2–B5 and B3–B5 and long B8–B5 and B9–B5 distances. These typical aspects of 4,1,10-*MC*<sub>2</sub>B<sub>10</sub> compounds are more fully discussed below.

The <sup>11</sup>B{<sup>1</sup>H} NMR spectrum of **7** was relatively uninformative (only three broad peaks with relative integrals 4:1:5), but importantly, there is only a single resonance in the <sup>31</sup>P{<sup>1</sup>H} NMR spectrum.<sup>6a</sup> The crystallographically determined molecular structure reveals a docosahedral cage with the phosphine ligands symmetrically disposed about an effective mirror plane passing through C1, Ni4, C10, and B11. This is clearly visible in Figure 5 center, a view of the nickel co-ordination sphere. As anticipated for such an orthogonal arrangement, the parameter  $\theta$  for compound **7** is 89.4°.

The <sup>11</sup>B{<sup>1</sup>H} NMR spectrum of **8** differs from that of **6** in that the relative integrals are slightly altered (2:2:1:1:2:2) and the whole spectrum is compressed and shifted to low frequency ( $\delta$  -4 to -18,  $\langle\delta(^{11}\text{B})\rangle = -11.4$ ), the latter anticipated for an anionic metallacarborane. In the <sup>1</sup>H spectrum the two cage CH resonances are again well separated,  $\delta$  5.1 and 2.1, and the different nature of the two cage {CH} units is further reinforced by very different chemical shifts in the <sup>13</sup>C{<sup>1</sup>H} spectrum,  $\delta$  79.0 and 42.4.

The docosahedral nature of the cage and the 4,1,10-RhC<sub>2</sub> heteroatom pattern are confirmed by a crystallographic study (Figure 6 and Table 5). This confirms that the anion has near C<sub>s</sub> symmetry about the plane defined by Rh4, C1, C10, and B11. In common with recent structural studies on related (ordered) 4,1,10-[M]C<sub>2</sub>B<sub>10</sub> species ([M] = CoCp, Ru(*p*-cymene), Nidppe),<sup>5a</sup> the B2–B5 and B3–B5 connectivities in **8** are very

**Figure 5.** Experimental conformations of the {*ML*<sub>2</sub>} fragments in **6** (left;  $\theta = 87.7^\circ$ ), **7** (center;  $\theta = 89.4^\circ$ ) and **8** (right;  $\theta = 104.2^\circ$ ).**Figure 6.** Perspective view of the anion of **8**, with thermal ellipsoids as for Figure 2.**Table 5.** Selected Interatomic Distances (Å) in the [4,4-cod-4,1,10-*closo*-RhC<sub>2</sub>B<sub>10</sub>H<sub>12</sub>]<sup>-</sup> Anion of **8**

C1–B2	1.527(5)	Rh4–B7	2.235(4)	B9–B11	1.729(5)
C1–B3	1.534(5)	Rh4–C10	2.302(3)	B9–B12	1.718(5)
C1–Rh4	2.177(3)	B5–B8	1.885(5)	C10–B12	1.706(5)
C1–B5	1.761(5)	B5–B9	1.915(5)	C10–B13	1.695(5)
B2–Rh4	2.266(4)	B5–B11	1.782(5)	B11–B12	1.774(5)
B2–B5	2.072(5)	B6–B9	1.763(5)	B11–B13	1.778(5)
B2–B6	1.813(5)	B6–C10	1.669(5)	B12–B13	1.743(5)
B2–B9	1.834(5)	B6–B12	1.756(5)	Rh4–C41	2.169(3)
B3–Rh4	2.350(4)	B7–B8	1.781(5)	Rh4–C42	2.167(3)
B3–B5	1.967(5)	B7–C10	1.674(4)	Rh4–C45	2.151(3)
B3–B7	1.858(5)	B7–B13	1.770(5)	Rh4–C46	2.158(3)
B3–B8	1.786(5)	B8–B11	1.756(5)	C41–C42	1.404(4)
Rh4–B6	2.284(4)	B8–B13	1.729(5)	C45–C46	1.406(4)

long, 2.072(5) and 1.967(5) Å, respectively, and the B8–B5 and B9–B5 distances long, 1.885(5) and 1.915(5) Å, respectively. Defining X1 as the midpoint of the C41=C42 bond and X2 as the midpoint of the C45=C46 bond, we note that the RhX<sub>2</sub> plane is slightly off perpendicular to the RhC1C10B11 plane, with  $\theta = 104.2^\circ$  (Figure 5 right). Pairwise across the effective mirror plane the B atom which is more closely trans to the alkene ligand is the more strongly bound to Rh, i.e., Rh4–B2 < Rh4–B3 and Rh4–B7 < Rh4–B6. The shortest Rh–B connectivity is to B7, and is accompanied by a small but clear trans influence in the Rh–C<sub>ene</sub> bonding, with Rh–C45,46 measurably shorter than Rh–C41,42.

The [N(PPh<sub>3</sub>)<sub>2</sub>]<sup>+</sup> cation in **8** is ordered, with N–P distances of 1.563(3) and 1.575(3) Å, and P–N–P = 145.05(18)°. Salt



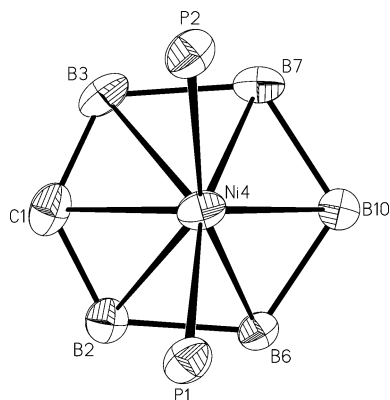


**Figure 7.** Experimental conformation of the  $\{NiP_2\}$  fragment in **9**.  $\theta = 90.0^\circ$ .

**8** cocrystallises with  $\frac{1}{2}CH_2Cl_2$ , disordered about a crystallographic inversion center.

**4,1,12- $MC_2B_{10}$  Compounds.** The nickelacarborane 4,4-(dppe)-4,1,12-*closo*- $NiC_2B_{10}H_{12}$ , **9**, is produced when the corresponding 4,1,10-isomer, compound **7**, is heated in refluxing toluene.<sup>6a</sup> Compound **9** has been characterized crystallographically.<sup>6a</sup> Although the structural determination suffers from partial disorder in one-half of the dppe ligand, it is nevertheless possible to define the conformation of the (major)  $NiP_2$  plane relative to the plane through  $NiC_1B_10B_{11}$  as  $\theta = 90.0^\circ$  (Figure 7).

**2. Conformations.** The crystallographic studies described above reveal what appears to be a clear preference for the conformations of  $\{ML_2\}$  fragments bonded to each of the four kinds of six-atom ligand faces in 13-vertex 4,1,*x*- $MC_2B_{10}$  metallocarboranes. For ligand type **III** (4,1,2- $MC_2B_{10}$ )  $\theta$  is  $61.1^\circ$  (compound **1**) and  $64.6^\circ$  (**2**). For ligand **IV** (4,1,6- $MC_2B_{10}$ ) we observe  $\theta = 148.7^\circ$  (**3**),  $134.6^\circ$ ,  $136.7^\circ$  (**4**), and  $115.1^\circ$  (**5**). Ligand type **V** (4,1,10- $MC_2B_{10}$ ) favors effectively perpendicular arrangements, with  $\theta = 87.7^\circ$  (**6**),  $89.4^\circ$  (**7**), and  $104.2^\circ$  (**8**), and this situation is maintained in the one example of ligand type **VI** (4,1,12- $MC_2B_{10}$ ), with  $\theta = 90.0^\circ$  in compound **9**. In this section we explore these conformations computationally.

In earlier studies of the conformations of  $\{ML_2\}$  fragments in icosahedral metallocarboranes we described the conformations as parallel ( $\parallel$ ) or perpendicular ( $\perp$ ) with respect to the mirror plane through the cage. When there are two adjacent cage C atoms in the ligating face, a  $\perp$  conformation is observed (**VII**, Chart 4).<sup>14b</sup> However, when the cage C atoms are nonadjacent, the alternative  $\parallel$  conformation is seen (**VIII**).<sup>27</sup> Finally, in the case of a single C atom in the ligating face, the conformation returns to  $\perp$  (**IX**).<sup>28</sup>

In all cases we rationalized these observations by the results of MO calculations (at the extended Hückel level) which revealed<sup>14</sup> that:

(1) in carborane ligands the frontier molecular orbitals are localized primarily on the B atoms in the open face;

(2) partitioning the electrons as  $d^{10}$ - $ML_2$  (and consequently neutral *nido*- $C_2B_9$  or monoanionic *nido*- $CB_{10}$  ligands), the metal fragment LUMO is an  $s-p_z$  hybrid (**X**, Chart 5) and the HOMO an in-plane  $d-p$  hybrid (**XI**), both reinforced away from the P

**Chart 4**

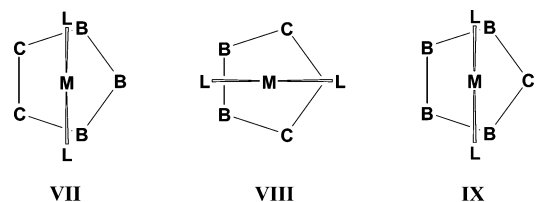
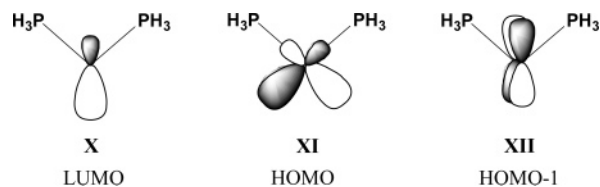


**Chart 5**



atoms. Clearly the metal LUMO has no conformational preference. The HOMO and HOMO-1 (**XII**), which is pure metal  $d$  character, have orthogonal conformational preferences; however, because of its hybridization, the HOMO has a greater interaction with the cage, and the overall conformation is set by the metal HOMO/cage LUMO interaction. For **VII** and **IX** as drawn above, the cage LUMO has a left-right nodal plane, and for **VIII** a top-bottom nodal plane, leading to  $\perp$  conformations in the cases of **VII** and **IX** and  $\parallel$  in the case of **VIII**;

(3) the magnitude and direction of the slip distortion of the  $\{ML_2\}$  fragment with respect to the cage is that which maximizes both sets of frontier orbital interactions.

These early calculations were useful in that they rationalized the observed conformations in terms of simple symmetry-based arguments, appropriate since in the icosahedron all vertices are of degree-five. This, however, is not the case in the 13-vertex dicosahedron and hencosahedron. Nevertheless, to allow optimal comparison with the icosahedral system we wanted to explore the conformations of  $ML_2$  fragments with respect to six-atom carborane rings in which the B and C atoms were equally connected, and thus initial calculations focused on the 18-electron heteroarene complexes,  $[(PH_3)_2PtC_2B_4H_6]^{2-}$  and  $[(PH_3)_2PtCB_5H_6]^{3-}$ . We attempted to optimize both  $\parallel$  and  $\perp$  structures for all three isomers of the  $C_2B_4$  species and for the  $CB_5$  species, using DFT.

When the two C atoms are adjacent, i.e., the analogue of the  $C_2B_{10}$  ligand type **III**, and structures were minimized in  $C_s$  symmetry, the  $\perp$  form (Figure 8, left) was found to be a minimum. The  $\parallel$  isomer (Figure 8, right) lies  $4.4 \text{ kcal mol}^{-1}$  above the  $\perp$  form, but the former is not a local minimum, having two imaginary frequencies which correspond to  $PH_3$  rotation. If the symmetry constraint is relaxed, however, a further minimum with one C atom eclipsed by a  $PH_3$  group (Figure 8, center) is located just  $+0.68 \text{ kcal mol}^{-1}$  above the  $\perp$  structure. Note that the minimum ( $\perp$ ) conformation corresponds to a form with  $\theta = 60^\circ$  and recall that in compounds **1** and **2** real examples of metallocarboranes incorporating the type **III**  $C_2B_{10}$  ligand measured  $\theta$  values were  $61.1^\circ$  and  $64.6^\circ$ .

In Figure 9 (left) is shown the minimum energy structure, optimized in  $C_s$  symmetry, for the  $[(PH_3)_2Pt(C_2B_4-1,3)]^{2-}$  species, the analogue of the platinumacarborane **3** containing the  $C_2B_{10}$  carborane type **IV**. This  $\parallel$  form is  $19.1 \text{ kcal mol}^{-1}$  more stable than the alternative  $\perp$  form (Figure 9, right) which corresponds to a transition state for  $\{Pt(PH_3)_2\}$  rotation. The  $\parallel$

(27) (a) Green, M.; Spencer, J. L.; Stone, F. G. A.; Welch, A. J. *J. Chem. Soc., Chem. Commun.* **1974**, 571. (b) Green, M.; Spencer, J. L.; Stone, F. G. A.; Welch, A. J. *J. Chem. Soc., Dalton Trans.* **1975**, 179. (c) Welch, A. J. *J. Chem. Soc., Dalton Trans.* **1975**, 1473.

(28) Carroll, W. E.; Green, M.; Stone, F. G. A.; Welch, A. J. *J. Chem. Soc., Dalton Trans.* **1975**, 2263.

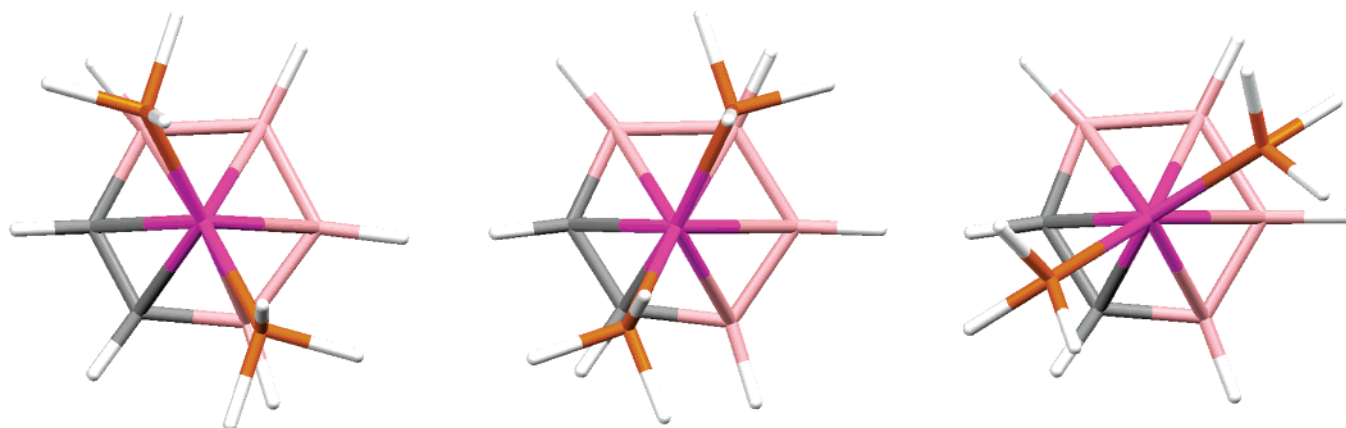


**Figure 8.** Computed [B3LYP/6-31G(d,p); Pt, SDD; P, SDD+d] conformations of  $[(PH_3)_2Pt(C_2B_4H_6-1,2)]^{2-}$ : (Left) Minimum energy. (Center) +0.68 kcal mol<sup>-1</sup>. (Right) +4.4 kcal mol<sup>-1</sup>.

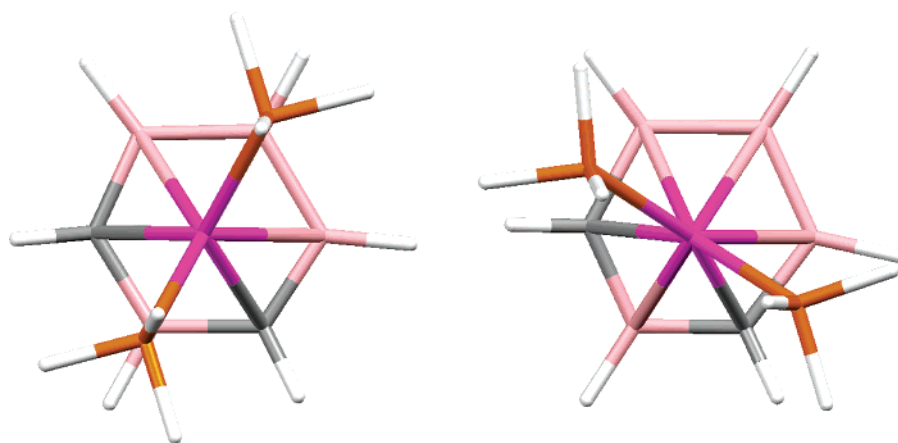


**Figure 9.** Computed [B3LYP/6-31G(d,p); Pt, SDD; P, SDD+d] conformations of  $[(PH_3)_2Pt(C_2B_4H_6-1,3)]^{2-}$ : (Left) Minimum energy. (Right) +19.1 kcal mol<sup>-1</sup>.

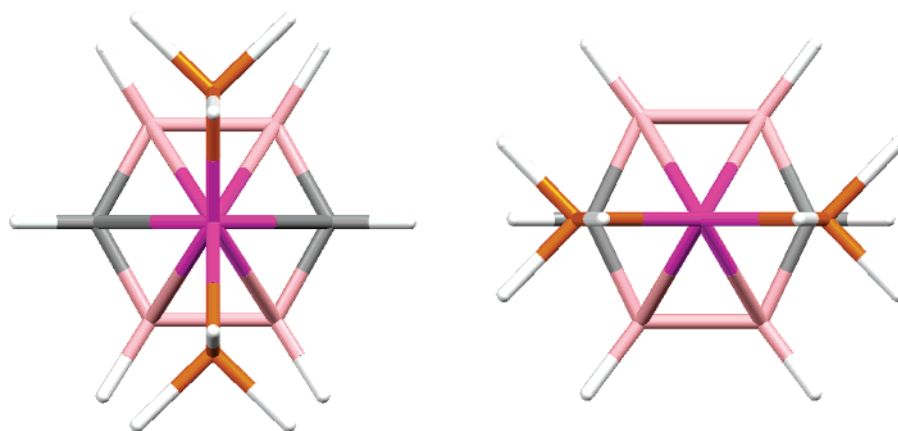


**Figure 10.** Computed [B3LYP/6-31G(d,p); Pt, SDD; P, SDD+d] conformations of  $[(PH_3)_2Pt(C_2B_4H_6-1,4)]^{2-}$ : (Left) Minimum energy. (Right) +22.0 kcal mol<sup>-1</sup>.

geometry of this model compound corresponds to  $\theta = 120^\circ$  in 4,1,6- $MC_2B_{10}$  metallacarboranes, in broad general agreement with experimental  $\theta$  values of  $148.7^\circ$  (compound **3**),  $134.6^\circ$  and  $136.7^\circ$  (compound **4**), and  $115.1^\circ$  (compound **5**).

There are two mirror planes of symmetry perpendicular to the  $C_2B_4-1,4$  heteroarene ring (the analogue of carborane type **V**), rendering the descriptors  $\parallel$  and  $\perp$  inappropriate and conferring potential  $C_{2v}$  symmetry on the  $[(PH_3)_2PtC_2B_4H_6]^{2-}$  ion. In  $C_{2v}$  symmetry the minimum structure (Figure 10, left)

has  $PtP_2$  and  $PtC_2$  planes orthogonal and lies 22.0 kcal mol<sup>-1</sup> below its rotamer in which the  $\{(PH_3)_2Pt\}$  fragment eclipses the C atoms (Figure 10, right). Again, the latter does not correspond to a local minimum, having two imaginary frequencies, one corresponding to  $\{Pt(PH_3)_2\}$  rotation and the other to  $PH_3$  rotation. In  $C_1$  symmetry exactly the same minimum as that shown in Figure 10 (left) is found, with the form of Figure 10 (right) collapsing to this by simple  $\{Pt(PH_3)_2\}$  rotation. The minimum structure corresponds to  $\theta = 90^\circ$  in metallacarboranes

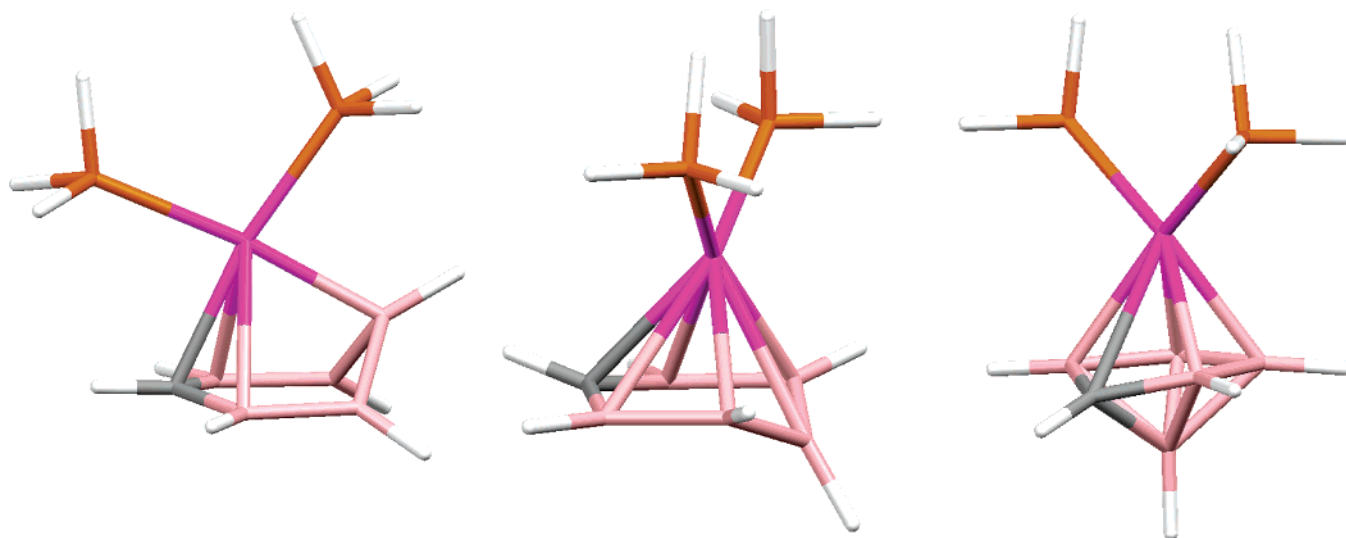


**Figure 11.** Results of attempted optimization [B3LYP/6-31G(d,p); Pt, SDD; P, SDD+d] of  $[(\text{PH}_3)_2\text{PtCB}_5\text{H}_6]^{3-}$ : (Left and center) with  $C_5$  symmetry imposed. (Right) with no imposed symmetry. Although the form on the right is  $\sim 50$  kcal mol $^{-1}$  more stable than the others, the original structure with a  $\text{CB}_5$  metallabonded ring has collapsed to give a distorted closo 7-vertex platynacarborane with only a  $\text{CB}_4$  metallabonded ring.

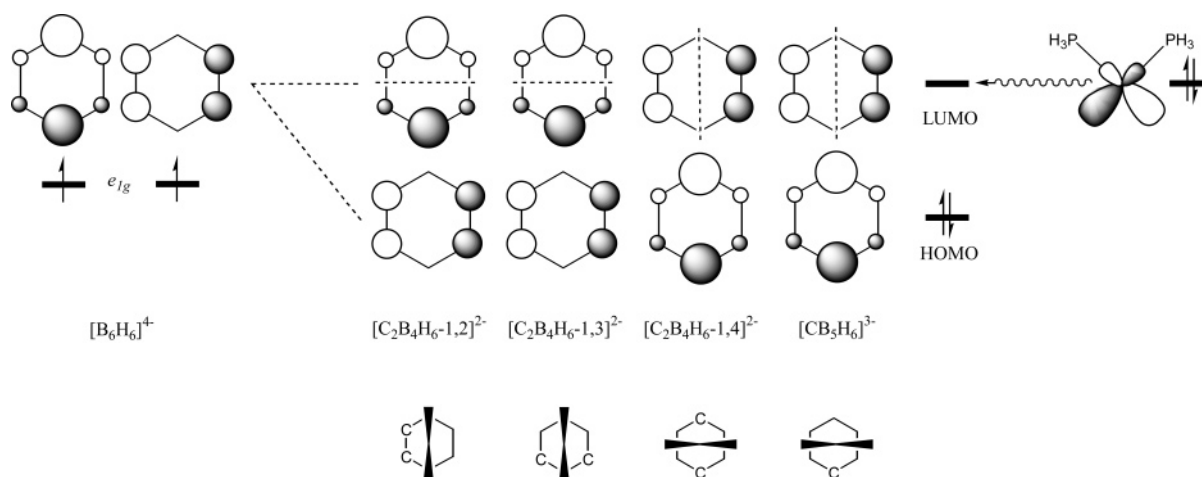


**Figure 12.** Qualitative representation of the splitting of the  $e_{1g}$  pair of MOs of  $[\text{B}_6\text{H}_6]^{4-}$  on carbon atom substitution, leading to (lower part) predicted conformations for the three isomers of  $[(\text{PH}_3)_2\text{PtC}_2\text{B}_4\text{H}_6]^{2-}$  and for  $[(\text{PH}_3)_2\text{PtCB}_5\text{H}_6]^{3-}$ .

incorporating the ligand type **V**, in excellent agreement with measured  $\theta$  values of 87.7°, 89.4°, and 104.2° in compounds **6**, **7**, and **8**, respectively.

Finally, we attempted to optimize  $\parallel$  and  $\perp$  forms of  $[(\text{PH}_3)_2\text{PtCB}_5\text{H}_6]^{3-}$  in which the  $\{(\text{PH}_3)_2\text{Pt}\}$  fragment is bonded to a  $\text{CB}_5$  ring, the analogue of carborane type **VI**. However, this species, a model for both 4,1,8- and 4,1,12- $\text{MC}_2\text{B}_{10}$  metallacarboranes (the latter represented experimentally by **9**), did not optimize as expected. If  $C_5$  symmetry is imposed, two structures are found, one  $\parallel$  and the other  $\perp$ , but neither is a minimum, each having two imaginary frequencies. The former (Figure 11, left) has the B atom opposite C substantially displaced out of the ring toward Pt, whereas in the latter (Figure 11, center) the  $\text{CB}_5$  ring has a chair conformation with the B opposite C bent away from Pt and an unrealistic B–H vector. In  $C_1$  symmetry, a minimum *is* found ( $\sim 50$  kcal mol $^{-1}$  below the two former structures), but this structure has collapsed from a nido species with a  $\text{CB}_5$  metallabonded ring into a distorted closo 7-vertex platynacarborane in which the metal is attached to only a  $\text{CB}_4$

ring. This form (Figure 11, right) has effective  $C_5$  symmetry but cannot be accessed without removal of the symmetry constraint.

A qualitative understanding of the  $[(\text{PH}_3)_2\text{PtC}_2\text{B}_4\text{H}_6]^{2-}$  conformations can be gained by considering how the degeneracy of the  $e_{1g}$  pair of  $\pi$  MOs of  $[\text{B}_6\text{H}_6]^{4-}$  is lifted upon carbon substitution (Figure 12). Since C is more electronegative than B, that orbital with the greater coefficient on C will be preferentially stabilized, becoming the HOMO of  $[\text{C}_2\text{B}_4\text{H}_6]^{2-}$  (or  $[\text{CB}_5\text{H}_6]^{3-}$ ). Conversely, the component of the  $e_{1g}$  pair with the smaller coefficient on C will form the LUMO of the heteroarene. By analogy with the previous work<sup>14</sup> on icosahedral platynacarboranes, we would expect the conformation to be set by the metal HOMO/heteroarene LUMO interaction, leading to the predicted conformations of  $[(\text{PH}_3)_2\text{PtC}_2\text{B}_4\text{H}_6]^{2-}$  shown in Figure 12, all of which are confirmed by calculation and supported by the crystallographic work on compounds **1–8**. This analysis also predicts a  $\perp$  conformation for  $[(\text{PH}_3)_2\text{PtCB}_5\text{H}_6]^{3-}$ . Although this model compound was not stable under optimiza-

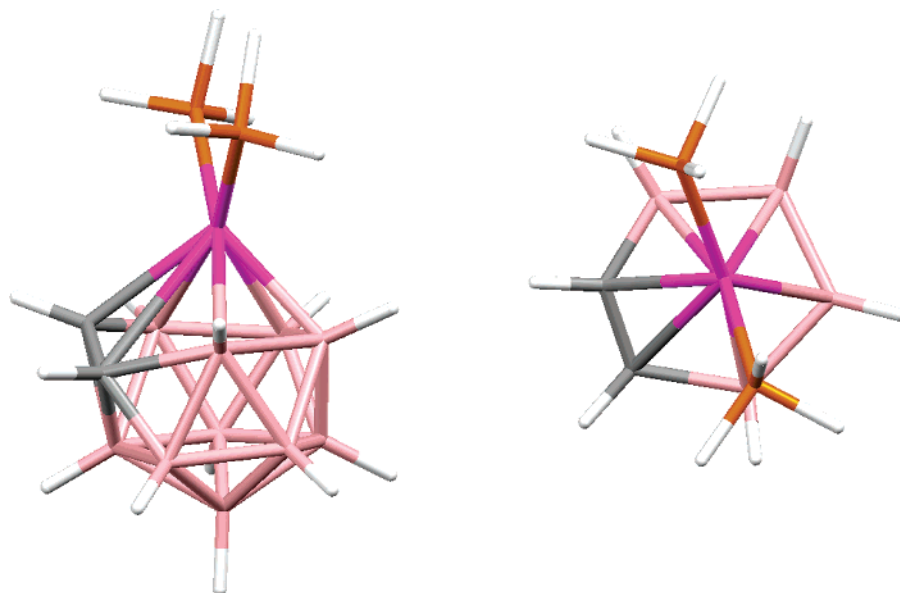


**Figure 13.** Optimized structure [B3LYP/6-31G(d,p); Pt, SDD; P, SDD+d] of 4,4-( $\text{PH}_3$ )<sub>2</sub>-4,1,2-*closo*- $\text{PtC}_2\text{B}_{10}\text{H}_{12}$  in  $C_1$  symmetry: (Left) Perspective view. (Right;) View showing the conformation.  $\theta = 68.4^\circ$ .

**Table 6.** Comparison of Selected Molecular Parameters ( $\text{\AA}$ , deg) in (Theoretical) 4,4-( $\text{PH}_3$ )<sub>2</sub>-4,1,2-*closo*- $\text{PtC}_2\text{B}_{10}\text{H}_{12}$  and (Experimental) 1,2-( $\text{CH}_2$ )<sub>3</sub>-4,4-( $\text{PMe}_2\text{Ph}$ )<sub>2</sub>-4,1,2-*closo*- $\text{PtC}_2\text{B}_{10}\text{H}_{10}$ , **1**

	( $\text{PH}_3$ ) <sub>2</sub> $\text{PtC}_2\text{B}_{10}\text{H}_{12}$	<sup>a</sup>
Pt4–C1	2.511	2.381(8)
Pt4–C2	2.906	2.626(8)
Pt4–B3	2.341	2.322(8)
Pt4–B6	2.312	2.310(7)
Pt4–B7	2.307	2.305(7)
Pt4–B10	2.253	2.265(7)
C2–B5	1.797	2.055(12)
Pt4–P1	2.335	2.3046(18)
Pt4–P2	2.353	2.3001(17)
P1–Pt4–P2	98.2	96.07(6)
$\theta$	68.0	60.8

<sup>a</sup> Data taken from ref 8.

tion, such a  $\perp$  conformation is displayed by the analogous real compound **9**.

While we have noted good general agreement between the experimental conformations in compounds **1–8** and those predicted for the appropriate models with  $C_2B_4$  heteroarene ligands, we recognize that these simple models are somewhat inappropriate in that, in the real systems, the two cage C atoms are not equivalent, one being of degree-four and the other degree-five. We have therefore extended the computational work to include optimizations of the 4,1,2-, 4,1,6-, and 4,1,10- isomers of the model 13-vertex metallacarborane, ( $\text{PH}_3$ )<sub>2</sub> $\text{PtC}_2\text{B}_{10}\text{H}_{12}$ , more closely to mimic the real systems. We have also optimized 4,4-( $\text{PH}_3$ )<sub>2</sub>-4,1,12-*closo*- $\text{PtC}_2\text{B}_{10}\text{H}_{12}$ , which could not satisfactorily be modeled by [( $\text{PH}_3$ )<sub>2</sub> $\text{PtC}_5\text{H}_6$ ]<sup>3-</sup>.

Figure 13 shows the structure optimized in  $C_1$  symmetry for 4,4-( $\text{PH}_3$ )<sub>2</sub>-4,1,2-*closo*- $\text{PtC}_2\text{B}_{10}\text{H}_{12}$ , and Table 6 provides a comparison of key molecular parameters for this optimized structure and for that of the analogous compound 1,2-( $\text{CH}_2$ )<sub>3</sub>-4,4-( $\text{PMe}_2\text{Ph}$ )<sub>2</sub>-4,1,2-*closo*- $\text{PtC}_2\text{B}_{10}\text{H}_{10}$ , **1**.<sup>8</sup> There is generally good agreement between calculated and found molecular structures, except that Pt4–C1 is somewhat overestimated in the calculation, by  $\sim 0.13 \text{ \AA}$ , and more seriously, C2–B5 is  $\sim 0.26 \text{ \AA}$  too short and Pt4–C2 is  $\sim 0.28 \text{ \AA}$  too long, in the computed model. Thus, while the experimental structure shows

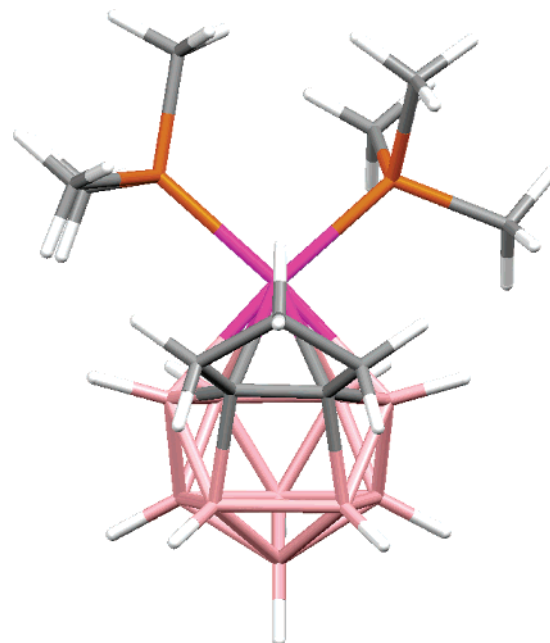


**Figure 14.** Hencicosahedral transition state computed [B3LYP/6-31G(d,p); Pt, SDD; P, SDD+d] for 1,2-( $\text{CH}_2$ )<sub>3</sub>-4,4-( $\text{PMe}_2$ )<sub>2</sub>-4,1,2-*closo*- $\text{PtC}_2\text{B}_{10}\text{H}_{10}$ .

a clear distortion toward hencicosahedron **II**, the computed structure is more like dicosahedron **I**, albeit with a very extended Pt4–C2 connectivity. Nevertheless, the computed conformation (right side of Figure 13), with  $\theta = 68.4^\circ$ , is in reasonable agreement with that found,  $\theta = 61.1^\circ$  (Figure 1).

Seeking further to understand these differences between computed and experimental results, we have also performed calculations on a much more representative species, 1,2-( $\text{CH}_2$ )<sub>3</sub>-4,4-( $\text{PMe}_2$ )<sub>2</sub>-4,1,2-*closo*- $\text{PtC}_2\text{B}_{10}\text{H}_{10}$ , in which the tether is included and a more realistic phosphine is used. In  $C_1$  symmetry this optimized with much the same cage structure as that found for the simplified species, 4,4-( $\text{PH}_3$ )<sub>2</sub>-4,1,2-*closo*- $\text{PtC}_2\text{B}_{10}\text{H}_{12}$ , i.e. with long Pt4–C2 (2.98  $\text{\AA}$ ) and short C2–B5 (1.83  $\text{\AA}$ ). However, in separate calculations we also noticed that artificially lengthening C2–B5 and concomitantly shortening Pt4–C2 to

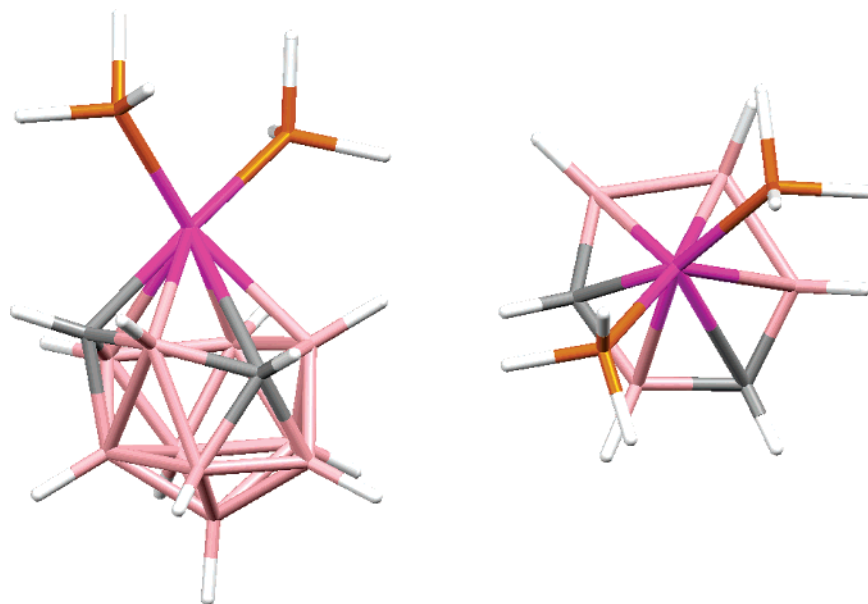


**Figure 15.** Optimized structure [B3LYP/6-31G(d,p); Pt, SDD; P, SDD+d] of 4,4-(PH<sub>3</sub>)<sub>2</sub>-4,1,6-*closo*-PtC<sub>2</sub>B<sub>10</sub>H<sub>12</sub> in C<sub>1</sub> symmetry: (Left) Perspective view. (Right) View showing the conformation.  $\theta = 141.1^\circ$ .

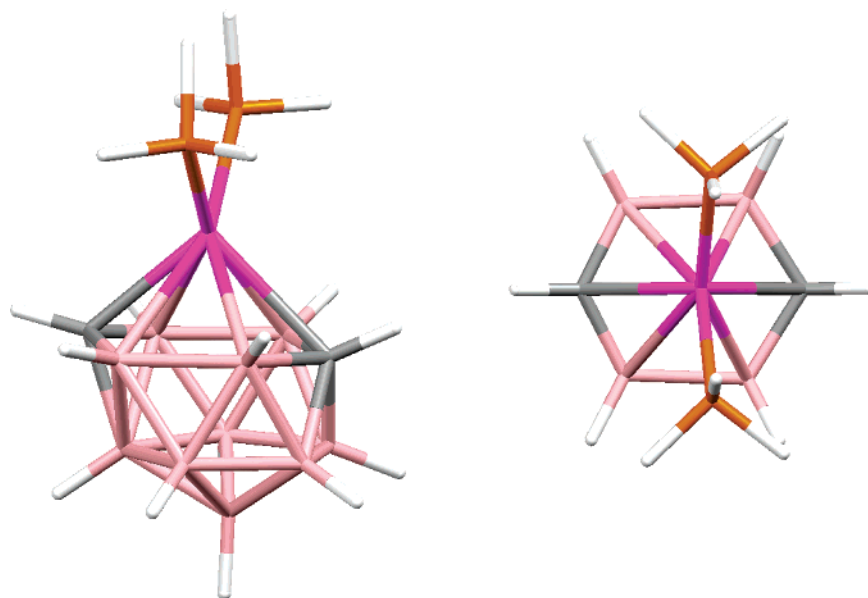


**Figure 16.** Optimized structure [B3LYP/6-31G(d,p); Pt, SDD; P, SDD+d] of 4,4-(PH<sub>3</sub>)<sub>2</sub>-4,1,10-*closo*-PtC<sub>2</sub>B<sub>10</sub>H<sub>12</sub> in C<sub>s</sub> symmetry: (Left) Perspective view. (Right) View showing the conformation.  $\theta = 90.0^\circ$  by symmetry.

values typical of those observed experimentally<sup>8</sup> results in only a marginally less stable molecule, perhaps suggesting that the observed structure is influenced by solid-state effects to some extent. Moreover, a relatively soft potential surface for this deformation is entirely consistent with the facile diamond–trapezium–diamond process we have previously proposed<sup>8</sup> to account for the fluxionality of compound **1** (and its Nidpe analogue) in solution, as evidenced by <sup>11</sup>B and <sup>31</sup>P NMR spectroscopy. In this process the dicosahedral ground-state structure transforms to the C<sub>s</sub> symmetric hicosahedron via, predominantly, C2–B5 extension and Pt4–C2 contraction. The hicosahedron could either collapse back to the original dicosahedron or to its mirror image in which C1–B9 shortened and Pt4–C1 lengthened. Since we could not arrest the fluxionality of **1** at low temperature we surmised that the activation

energy for the process was unlikely to be greater than ~10 kcal mol<sup>-1</sup>.<sup>29</sup> For 1,2-(CH<sub>2</sub>)<sub>3</sub>-4,4-(PMe<sub>3</sub>)<sub>2</sub>-4,1,2-*closo*-PtC<sub>2</sub>B<sub>10</sub>H<sub>10</sub> a hicosahedral transition state was subsequently located 8.3 kcal mol<sup>-1</sup> above the ground-state structure, entirely in keeping with this suggestion. This transition state is shown in Figure 14. It has nearly perfect C<sub>s</sub> cage symmetry, broken only for the molecule as a whole by a staggered arrangement of the {Pt(PMe<sub>3</sub>)<sub>2</sub>} unit. Pt4–C2 (= Pt4–C1) is 2.52 Å and C2–B5 (= C1–B9) is 2.46 Å. Reassuringly, a similar hicosahedral transition state was also located for the simplified model compound, 4,4-(PH<sub>3</sub>)<sub>2</sub>-4,1,2-*closo*-PtC<sub>2</sub>B<sub>10</sub>H<sub>12</sub>, 7.5 kcal mol<sup>-1</sup>

(29) Abel, E. W.; Bhargava, J. K.; Orrell, K. G. *Prog. Inorg. Chem.* **1984**, 32, 1.

(30) *The United Kingdom Chemical Database Service*; Fletcher, D. A.; McMeeking, R. F.; Parkin, D. J. *Chem. Inf. Comput. Sci.* **1996**, 36, 746.

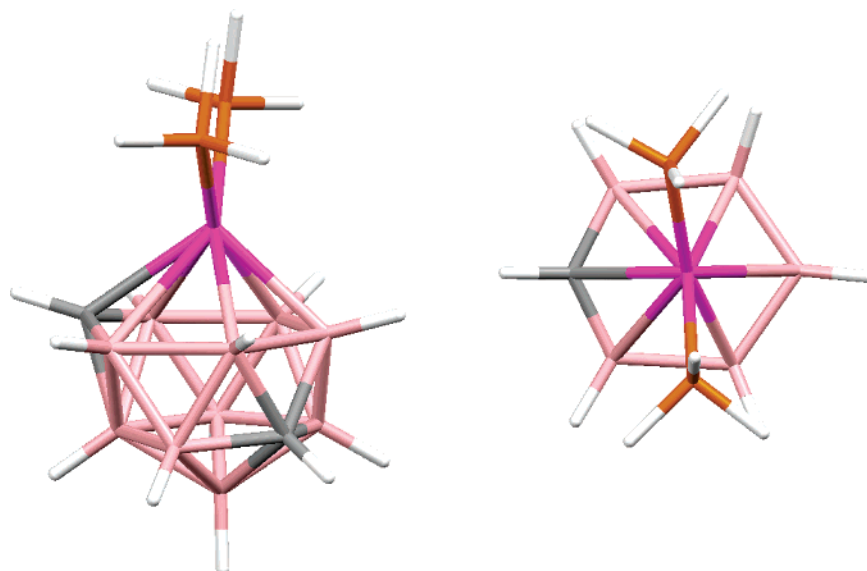


**Figure 17.** Optimized structure [B3LYP/6-31G(d,p); Pt, SDD; P, SDD+d] of 4,4-( $PH_3$ )<sub>2</sub>-4,1,12-*closo*-PtC<sub>2</sub>B<sub>10</sub>H<sub>12</sub> in  $C_1$  symmetry: (Left) Perspective view. (Right) View showing the conformation.  $\theta = 84.4^\circ$ .

**Table 7.** Comparison of Selected Molecular Parameters ( $\text{\AA}$ , deg) in (Theoretical) 4,4-( $PH_3$ )<sub>2</sub>-4,1,6-*closo*-PtC<sub>2</sub>B<sub>10</sub>H<sub>12</sub> and (Experimental) 4,4-( $PMe_2Ph$ )<sub>2</sub>-4,1,6-*closo*-PtC<sub>2</sub>B<sub>10</sub>H<sub>12</sub>, **3**

	( $PH_3$ ) <sub>2</sub> PtC <sub>2</sub> B <sub>10</sub> H <sub>12</sub>	<b>3</b>
Pt4–C1	2.180	2.1652(12)
Pt4–B2	2.499	2.4438(15)
Pt4–B3	2.445	2.3961(14)
Pt4–C6	2.956	2.8131(13)
Pt4–B7	2.244	2.2631(14)
Pt4–B10	2.475	2.3692(14)
Pt4–P1	2.300	2.2710(3)
Pt4–P2	2.378	2.3129(4)
P1–Pt4–P2	97.25	92.363(14)
$\theta$	141.3	148.4

above the ground-state structure, implying that, at least in terms of the activation barrier, these simplified models represent appropriate approximations.

The structure calculated (in  $C_1$  symmetry) for 4,4-( $PH_3$ )<sub>2</sub>-4,1,6-*closo*-PtC<sub>2</sub>B<sub>10</sub>H<sub>12</sub> is shown in Figure 15 and is in good agreement with that already described for compound **3**. Table 7 compares key molecular parameters. The greatest discrepancies are in Pt4–C6 and Pt4–B10 separations, too long in the calculations by  $\sim 0.15$  and  $0.10$   $\text{\AA}$ , respectively. Nevertheless, the very long Pt–C6 distance and severe buckling of the C<sub>2</sub>B<sub>4</sub> carborane ligand face are both faithfully reproduced in the calculation, which also successfully predicts (in the correct sense) unequal Pt–P distances. The calculated ( $\theta = 141.1^\circ$ ) and observed ( $\theta = 148.7^\circ$ ) conformations also agree well, and it is particularly noteworthy that the conformation of this platinumcarborane is much better reproduced in the model using a C<sub>2</sub>B<sub>10</sub> ligand rather than the simplified (heteroarene) C<sub>2</sub>B<sub>4</sub> ligand.

In Figure 16 are perspective and plan views of the structure of 4,4-( $PH_3$ )<sub>2</sub>-4,1,10-*closo*-PtC<sub>2</sub>B<sub>10</sub>H<sub>12</sub> optimized in  $C_s$  symmetry, while Table 8 lists selected molecular parameters. The appropriate comparison here would be with the structure determined for **6**, but unfortunately, as noted above, this suffers from crystallographic disorder which masks subtle variations within the cage. Thus, for example, while the computational study predicts different Pt–C distances (Pt4–C1 2.291  $\text{\AA}$ , Pt4–

**Table 8.** Selected Molecular Parameters ( $\text{\AA}$ , deg) for the  $C_s$  Symmetric Optimized Structure of 4,4-( $PH_3$ )<sub>2</sub>-4,1,10-*closo*-PtC<sub>2</sub>B<sub>10</sub>H<sub>12</sub>

C1–B2	1.533	Pt4–B6	2.344	B9–B11	1.770
C1–Pt4	2.315	Pt4–C10	2.497	B9–B12	1.750
C1–B5	1.783	B5–B9	1.897	C10–B12	1.680
B2–Pt4	2.412	B5–B11	1.766	B11–B12	1.790
B2–B5	2.022	B6–B9	1.770	B12–B13	1.760
B2–B6	1.927	B6–C10	1.682	Pt4–P1	2.334
B2–B9	1.793	B6–B12	1.773	P1–Pt4–P1A	97.28

**Table 9.** Selected Molecular Parameters ( $\text{\AA}$ , deg) for the  $C_1$  Symmetric Optimized Structure of 4,4-( $PH_3$ )<sub>2</sub>-4,1,12-*closo*-PtC<sub>2</sub>B<sub>10</sub>H<sub>12</sub>

C1–B2	1.529	Pt4–B6	2.250	B8–B11	1.746
C1–B3	1.539	Pt4–B7	2.297	B8–B13	1.756
C1–Pt4	2.384	Pt4–B10	2.301	B9–B11	1.762
C1–B5	1.784	B5–B8	1.901	B9–C12	1.683
B2–Pt4	2.500	B5–B9	1.886	B10–C12	1.704
B2–B5	2.007	B5–B11	1.768	B10–B13	1.770
B2–B6	1.920	B6–B9	1.770	B11–C12	1.722
B2–B9	1.770	B6–B10	1.847	B11–B13	1.786
B3–Pt4	2.451	B6–C12	1.679	C12–B13	1.692
B3–B5	2.015	B7–B8	1.784	Pt4–P1 <sup>a</sup>	2.338
B3–B7	1.930	B7–B10	1.794	Pt4–P2 <sup>a</sup>	2.341
B3–B8	1.783	B7–B13	1.752	P1–Pt4–P2	95.25

<sup>a</sup> P1 trans to B3–B7 and P2 trans to B2–B6, as in compound **9**.

C10 2.484  $\text{\AA}$ ), in the diffraction study C1 and C10 are disordered about a crystallographic  $C_2$  axis, and a single, average Pt–C distance is measured, 2.357(2)  $\text{\AA}$ . Nevertheless, the overall comparison between experimental and computational structures is clearly very good. In the crystallographic study  $\theta = 87.7^\circ$ , while in the computational study it is required to be precisely  $90.0^\circ$  by the  $C_s$  symmetry imposed.

Figure 17 shows the structure optimized for 4,4-( $PH_3$ )<sub>2</sub>-4,1,12-*closo*-PtC<sub>2</sub>B<sub>10</sub>H<sub>12</sub>, and Table 9 lists important derived molecular parameters. Although we do not have an experimental 4,1,12-*closo*-PtC<sub>2</sub>B<sub>10</sub> compound with which to compare this computational result (the obvious precursor, compound **6**, is relatively unstable and does not survive even gentle thermolysis), it is encouraging that the main features of the only two 4,1,12-*MC*<sub>2</sub>B<sub>10</sub> species to have been crystallographically characterized,

4-Cp\*-4,1,12-*closo*-CoC<sub>2</sub>B<sub>10</sub>H<sub>12</sub><sup>10k</sup> (Cp\* =  $\eta$ -C<sub>5</sub>Me<sub>5</sub>) and 4,4-dppe-4,1,12-*closo*-NiC<sub>2</sub>B<sub>10</sub>H<sub>12</sub>, **9**,<sup>6a</sup> viz. long B2–B5, B3–B5, and B5–B9 distances, are reproduced by the calculation. Moreover, the calculated  $\theta$  value, 84.4°, is in excellent agreement with that measured for **9**, 90.0°.

### Conclusions

Recent developments in supraicosahedral metallocarborane chemistry have allowed access to homologous series of compounds with four different types of six-atom faces presented to the metal fragment; including the three new compounds reported herein, we now have a total of nine crystallographically characterized examples of species with {ML<sub>2</sub>} fragments bound to these six-atom faces. In these species clear patterns are visible in the conformations of the {ML<sub>2</sub>} fragments with respect to the carborane ligand.

Initially we explored these conformations for C<sub>2</sub>B<sub>4</sub> carborane faces by DFT calculations on the model compounds [(PH<sub>3</sub>)<sub>2</sub>PtC<sub>2</sub>B<sub>4</sub>H<sub>6</sub>]<sup>2-</sup> and successfully rationalized the results by qualitative MO arguments. Unfortunately, analogous calculations on [(PH<sub>3</sub>)<sub>2</sub>PtCB<sub>5</sub>H<sub>6</sub>]<sup>3-</sup> as a model compound with a CB<sub>5</sub> ligand face were unsuccessful. However, further calculations on the polyhedral model compounds (PH<sub>3</sub>)<sub>2</sub>PtC<sub>2</sub>B<sub>10</sub>H<sub>12</sub> successfully reproduced the observed conformations for all four types of carborane ligand.

In some cases the calculations led to apparent overestimation of Pt–C distances, and in investigating this for the realistic model compound, 1,2-(CH<sub>2</sub>)<sub>3</sub>-4,4-(PMe<sub>3</sub>)<sub>2</sub>-4,1,2-*closo*-PtC<sub>2</sub>B<sub>10</sub>H<sub>10</sub>, we were able to compute a low activation energy for intercon-

version of dicosahedral enantiomers, consistent with our inability to arrest the fluxionality of 1,2-(CH<sub>2</sub>)<sub>3</sub>-4,4-(PMe<sub>2</sub>Ph)<sub>2</sub>-4,1,2-*closo*-PtC<sub>2</sub>B<sub>10</sub>H<sub>10</sub>. Calculations on (PH<sub>3</sub>)<sub>2</sub>PtC<sub>2</sub>B<sub>10</sub>H<sub>12</sub> also allowed the structure of the experimentally unavailable 4,1,12-PtC<sub>2</sub>B<sub>10</sub> cluster to be explored and proved superior to experiment in the case of the severely crystallographically disordered 4,1,10-PtC<sub>2</sub>B<sub>10</sub> species.

**Acknowledgment.** We thank the EPSRC (D.E., S.E.), the Carnegie Trust (R.D.McI.), and the Robert A. Welch Foundation (B.E.H., T.D.McG.; Grant AA-0006) for support. At Heriot-Watt we thank Dr. A. S. F. Boyd for NMR spectra, Mr. G. Smith for mass spectra, Ms. C. Graham for elemental analysis, and we acknowledge provision of the diffractometer from EPSRC Grant GR/R99065. At Baylor the diffractometer was purchased with funds from the National Science Foundation Major Research Instrumentation Programme (Grant CHE-0321214). We acknowledge use of the EPSRC Chemical Database Service at Daresbury.<sup>30</sup> V.S. is the recipient of a Socrates scholarship from the Philipps-Universität Marburg, Germany.

**Supporting Information Available:** Full details of the crystallographic analyses of **3**, **6**, and **8**· $\frac{1}{2}$ CH<sub>2</sub>Cl<sub>2</sub> as a CIF; Cartesian coordinates of all model compounds shown in Figures or otherwise discussed in the text along with complete ref 23 as a text file. This material is available free of charge via the Internet at <http://pubs.acs.org>

JA067698M